The University of Maine
DigitalCommons@UMaine

Electronic Theses and Dissertations | Fogler Library

Fall 12-20-2020

An Experimental Investigation of Alternative Wave Attenuation Mechanisms for a Modular Breakwater

Richard Perry
University of Maine, richard.a.perry@maine.edu

Follow this and additional works at: https://digitalcommons.library.umaine.edu/etd

 Part of the Civil Engineering Commons, and the Environmental Engineering Commons

Recommended Citation

Perry, Richard, "An Experimental Investigation of Alternative Wave Attenuation Mechanisms for a Modular Breakwater" (2020). *Electronic Theses and Dissertations*. 3370.
https://digitalcommons.library.umaine.edu/etd/3370

This Open-Access Thesis is brought to you for free and open access by DigitalCommons@UMaine. It has been accepted for inclusion in Electronic Theses and Dissertations by an authorized administrator of DigitalCommons@UMaine. For more information, please contact um.library.technical.services@maine.edu.

AN EXPERIMENTAL INVESTIGATION OF ALTERNATIVE WAVE ATTENUATION MECHANISMS FOR A MODULAR BREAKWATER

By

Richard Perry

B.S. University of Maine, 2018

A THESIS

Submitted in Partial Fulfillment of the

Requirements for the Degree of

Master of Science

(in Civil Engineering)

The Graduate School

The University of Maine

December 2020

Advisory Committee:

Kimberly Huguenard, Assistant Professor of Civil Engineering, Advisor

Anthony M. Viselli, Research Assistant Professor and Manager of Offshore Testing and Design, Advanced Structures and Composites Center, Co-Advisor

Lauren Ross, Assistant Professor of Civil Engineering, Co-Advisor

© 2020 Richard A. Perry

All Rights Reserved

AN EXPERIMENTAL INVESTIGATION OF ALTERNATIVE TURBULENT GENERATING WAVE ATTENUATION MECHANISMS FOR A MODULAR BREAKWATER

By Richard Perry

Thesis Advisor: Dr. Kimberly Huguenard

An Abstract of the Thesis Presented
in Partial Fulfillment of the Requirements for the
Degree of Master of Science
(in Civil Engineering)
December 2020

Global warming and sea level rise threaten to render traditional coastal protection structures as less effective. Floating breakwaters offer the advantages of adapting to rising sea level, allowing important material transport to occur, and being able to deploy and adapt to varying environmental conditions (seabed, depth, etc.). Traditional floating breakwaters typically consist of reflective concrete structures that are limited semi-sheltered locations. This research aimed to construct floating breakwaters out of lightweight materials with a smaller footprint while utilizing alternative attenuation mechanisms.

Three breakwaters consisting of a box, beach, and pipe designs were constructed at 1:40 scale and tested in a Wind and Wave Basin located in the Advanced Structures and Composites Center at the University of Maine. All three were designed to be constructed of lightweight composite sandwich material as opposed to concrete. The pipe breakwater was designed to utilize drag and vortex shedding as wave attenuation mechanisms, while the beach was designed to utilize wave breaking to induce turbulence.

The target operation environment for the breakwaters was a period of 3-6 s, and within this range, the beach breakwater was able to attenuate 50% of the energy up to a period of 5.5 s. This was comparable to the box, which attenuated 50% of the energy up to a period of 7.5 s. The beach was able to utilize an alternative to reflection to attenuate wave energy, with greater than 50% of the attenuation coming from dissipation. The beach also had the advantage of being half the full-scale width of the box, 8.56 m wide compared to 16.9 m for the box. The overall weight of the full scale box breakwater constructed from composite sandwich materials was 88% less (200 metric tons vs 1548 metric tons) than the same design made of conventional concrete. This work demonstrates the possibility to reduce the size, weight, and attenuation mechanism of a breakwater, while maintaining its overall effectiveness.

ACKNOWLEDGEMENTS

I would like to thank the Engineer Research and Development Center (ERDC) for funding this project and making this possible. I would like to thank the Advanced Structures and Composites Center and the Civil Engineering Department at the University of Maine for taking a chance on me and allowing me to do this research. It is important that I thank the Wind and Wave Lab team at the Composites Center. Chris Allen for your patient help with ANSYS, Matt Fowler for providing guidance and technical input when needed, Matt Cameron for running the lab and providing practical input about model testing, Peter Jalbert for remaining patient with me in design and model construction phases, and all the undergrad staff that help run and setup tests every day.

I would like to thank Dr. Lauren Ross for always lending an ear and being there if I needed help. Her passion and energy is one of the driving factors in what got me here today. Dr. Anthony Viselli for taking me under his wing in the early stages of this journey and patiently imparting some of his floating structure wisdom and vision on me. Dr. Kim Huguenard for her unwavering support and patience with me. There were several challenges along the way but she remained positive and kept me focused on the task at hand. Without the support, energy, positivity, and patience of these three individuals this research would not have been possible.

I would also like to thank some of the many peers that helped me along the way. William West for help with mooring line analysis and Hannah Allen for our continued struggle learning ANSYS and as a valuable sounding board. I would especially like to thank Taylor Bailey who started and finished this process with me. Her knowledge,

willingness to help and to listen provided stability and sanity that was much needed. Without her, I do not know if I would have made it through this process.

Last but certainly not least, I want to thank my family. My two boys Dylan and Owen for being patient with me when I was busy. My mom, Sharon Perry for volunteering to move 200 miles to watch the baby (Owen) so I could afford to get my Master's Degree. My wonderful wife, Brittani Perry. Her encouragement and support, both financial and mental, made this journey possible. Her unwavering belief that I could do this and that it would provide a great benefit to my career and our family provided much needed encouragement along this incredible journey.

TABLE OF CONTENTS

LIST OF TABLES

LIST OF FIGURES

LIST OF NOMENCLATURE

a	=	total fluid flow
$\bar{a}$	=	time averaged fluid flow component
$\tilde{a}$	=	wave induced periodic flow component
a'	=	turbulent flow component
C_d	=	dissipation coefficient
C_r	=	reflection coefficient
C_t	=	transmission coefficient
χ^2	=	chi-squared value from table
d	=	water depth
D	=	draft
df	=	frequency step
D_{ia}	=	diameter
D/d	=	draft to depth ratio
E_d	=	dissipated energy
E_i	=	incident energy
E_r	=	reflected energy

E_{tot}	=	total energy
η	=	variance of the power spectral density
EA	=	stiffness
f_s	=	wave frequency
g	=	gravitational constant
H_i	=	incident wave height
H_t	=	transmitted wave height
L	=	wavelength
L_c	=	characteristic length
L_f	=	length of frequency spectrum
m_{tot}	=	total mass of the structure
M	=	half width of the window
N_{pts}	=	number of data points in a time series
ν	=	kinematic viscosity
ν_f	=	degrees of freedom in spectral analysis
Re	=	Reynolds number
ρ	=	density of water

$s^2(f)$	=	standard deviation of the frequency spectrum
St	=	Strouhal number
T	=	wave period
u	=	along channel fluid velocity
$u_i' u_j'$	=	Reynolds stress
V_i	=	submerged volume of section
V_{tot}	=	total submerged volume
W	=	breakwater width

LIST OF ACRONYMS AND ABBREVIATIONS

$Aqwa$	=	ANSYS Aqwa
CB_i	=	center of buoyancy of a section
$C_{CI\ Upper}$	=	upper confidence interval coefficient
$C_{CI\ Lower}$	=	lower confidence interval coefficient
CI_{lower}	=	lower confidence interval (5%)
CI_{upper}	=	upper confidence interval (95%)
COB	=	center of buoyancy
COG	=	center of gravity
$Cosh$	=	hyperbolic cosine
fft	=	fast Fourier transform
Hz	=	hertz
IMO	=	International Maritime Organization
kg	=	kilogram
kN	=	kilonewton
m	=	meters
mm	=	millimeters

MKE	=	mean kinetic energy
N	=	newton
$PIANC$	=	Permanent International Association of Navigation Congresses
pvc	=	polyvinyl chloride
PSD	=	power spectral density
rad	=	radians
s	=	seconds
$Sinh$	=	hyperbolic sine
$SS3$	=	sea state 3
TKE	=	turbulent kinetic energy
Vdc	=	direct current voltage
WKE	=	wave kinetic energy

CHAPTER 1

INTRODUCTION

1.1. Motivation

Sea level rise from climate change threatens our coasts and seaports. Approximately 80% of global trade by volume and 70% of trade by value is carried by sea (United Nations, 2018). A 100 year storm, a severe event that has a 1% chance of happening every year, is typically used in design practice for coastal and seaport protection. Increasing frequency of storms and the additional inland vulnerability caused by rises in sea level, some models predict that a 100 year storm will increase to a 4-8% chance in a year (Kopp, et al., 2014). One form of coastal and seaport protection is the use of breakwaters. Fixed bottom breakwaters, though highly effective in present day conditions, require continued maintenance and adaptation for rising sea levels. The overarching goal of this thesis is to create resilient breakwater designs that are capable of adjusting to changes in water level, while providing coastal and seaport protection in typical coastal environments.

1.2. Scope and Research Objectives

This research seeks to provide a floating breakwater design that is lighter than traditional concrete breakwaters, smaller in footprint and easily constructed for rapid deployment. The research objectives are to (1) design floating breakwaters out of a composite material that will use turbulence rather than wave reflection to attenuate wave energy, (2) evaluate the wave attenuation capacity and loading on mooring lines and (3) analyze the effectiveness of turbulence as a mechanism to reduce wave energy, wave reflection and breakwater size.

1.3. Floating Breakwaters

Floating breakwaters are an alternative to fixed bottom breakwaters for providing sheltered areas from an incident wave field and have a historic past. In World War II, temporary harbors called Mulberry Harbors, were established using both fixed and floating breakwaters in an effort to offload large cargo and transport ships with soldiers and supplies in the absence of friendly deep water ports (Lochner, Faber, & Penney, 1948). The construction of the Mulberry Ports consisted of Phoenix breakwaters, which were large concrete caissons that were floated across the channel and ballasted in place (Carr, 1951). These were coupled with the Bombardon floating breakwater which was a steel structure in the shape of a Maltese cross (Lochner, Faber, & Penney, 1948).

1.3.1. Types of Floating Breakwaters

Floating breakwaters can be broken up into five different categories: box, pontoon, frame, mat, and tethered float (Figure 1a).

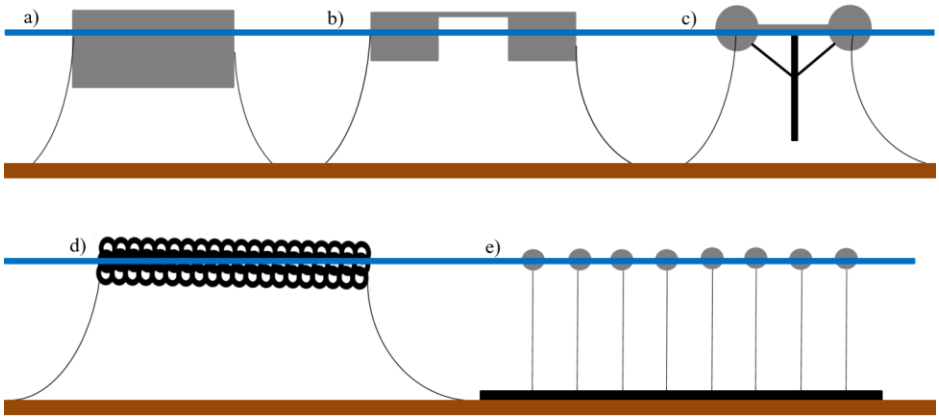

Figure 1. The five main categories of floating breakwaters, box (a), pontoon (b), frame (c), mat (d), and tethered (e). The mean sea level represented by the blue line and the sea floor by the brown line.

The box type is the most common type because of its simple design and dual functionality. Marinas often contain floating box breakwaters to provide a sheltered area,

in addition to functioning as a pier or dock for boats. The box primarily uses reflection for wave attenuation.

The pontoon breakwater (Figure 1b) is comprised of two box breakwaters rigidly connected by a platform and is similar to a pontoon or catamaran boat. Extending the distance between the pontoons allows for greater moment of inertia and stability without increasing the mass (Dai, Wang, Utsunomiya, & Duan, 2018). Pontoon breakwaters use reflection as the primary attenuation mechanism with the added benefit of dissipation that occurs between the two pontoons. In a theoretical investigation, it was determined that the amount of reflection depends strongly on the draft, width and spacing of the pontoons, in addition to the mooring line stiffness (Williams, Lee, & Huang, 2000).

A frame floating breakwater (Figure 1c) is a box or pontoon style breakwater with a rigid frame connected to the structure that extends into the water column. The upper part of the structure reflects wave energy while the extended portion induces a second mode of wave attenuation. For example, a wave fence of pressure treated timber attached to the bottom of a concrete pontoon (Allyn, Watchorn, Jamieson, & Yang, 2004). The spacing of the timber in the fence allows water to pass through while generating turbulence to dissipate energy.

A mat floating breakwater (Figure 1d) is commonly made of a large number floating scrap tires connected together. This structure dissipates energy by creating friction along the wetted surface as well as disrupting particle orbits (Dai, Wang, Utsunomiya, & Duan, 2018). The width of the tire-floating breakwater has to be at least 80% of the wavelength to achieve a transmission coefficient (C_t), which is the ratio of the

transmitted wave height divided by the incident wave height ($C_t=H_t/H_i$), of 0.5 (Giles & Sorensen, 1978).

A tethered float breakwater (Figure 1e) has a large number of smaller floats attached to the sea floor or a submerged structure via tethers. With this type of structure, reflection is a minor contributor, with the primary attenuation mechanism being drag (Seymour & Hanes, 1979).

1.3.2. Advantages and Limitations of Floating Breakwaters

Floating breakwaters have several advantages over fixed bottom breakwaters, such as independence of bathymetry or sea floor composition (Figure 2) and cost effectiveness once the water depth is greater than 6.1 m (McCartney, 1985).

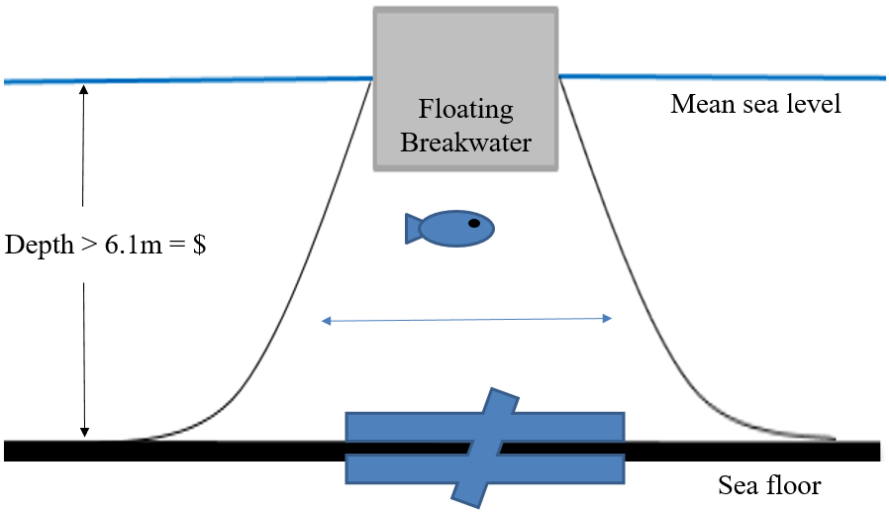

Figure 2. Advantages of floating compared to fixed bottom breakwaters. Including independence of sea floor composition, being more economical in depths greater than 6.1 m, and allowing aquatic organisms and sediment transport.

They can be modular such that the system can be altered with changing wave climates and can be used as temporary structures, creating a sheltered wave environment such as a temporary harbor for offloading ships or construction of coastal structures.

Floating breakwaters have the advantage of minimal interruption of natural processes, like sediment transport and the passage of aquatic organisms (Figure 2). For these reasons, floating breakwaters have been researched as an attractive option for coastal protection. Though, according to Sorenson (2006), floating breakwaters are typically only effective in semi-sheltered wave environments with periods of less than 2 to 3 seconds (Figure 3).

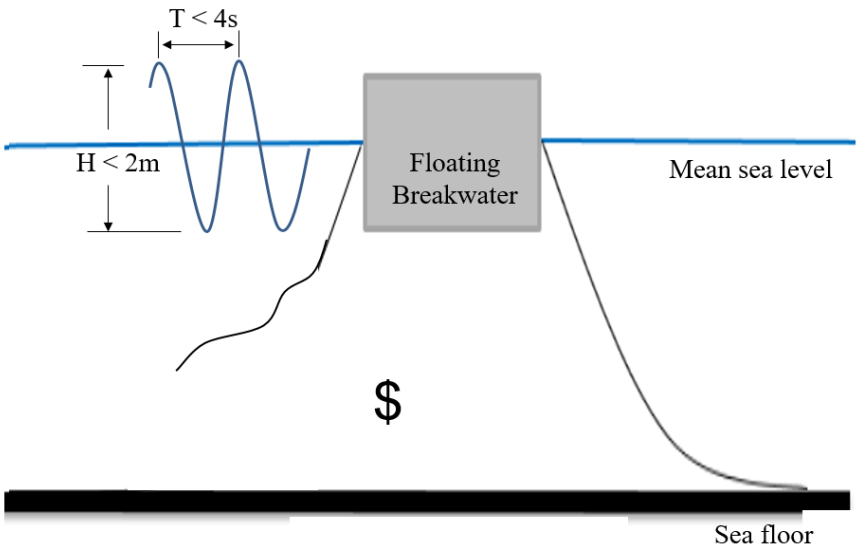

Figure 3. Disadvantages of floating breakwaters including increased maintenance, mooring failure, and performance limitations.

Coastal environments tend to experience wave periods ranging from 3 to 6 seconds more than 50% of the time (Briggs, 2001). Other disadvantages include increased maintenance over the life of the structure, including the possibility of some or all mooring lines failing which could cause substantial damage to other structures of vessels in the area (Figure 3).

The most commonly used floating breakwater is a box or single pontoon. Hales (1981) showed that either structure requires a width to wavelength ratio of 0.3 to be

effective. Floating breakwaters are most often evaluated by the transmission coefficient (C_t) within a regular wave environment. A breakwater is arbitrarily deemed effective if waves are attenuated by 50%, yielding a C_t of 0.5, though effectiveness could be defined by local constraints in implementation. Nonetheless, in order for floating breakwaters to classically be considered effective coastal protection measures, the structures would have to be very large (e.g. over 14 m wide for a depth of 10 m and a period of 6 s). The largest disadvantages of floating breakwaters are the size required to effectively attenuate coastal wave environments, in addition to reflection of the incident wave field. Wave reflection can be problematic, causing enhanced wave action that is both detrimental to naval passage and nearby coastlines through erosion. This research seeks to understand if alternative wave attenuation mechanisms, other than wave reflection, can be used in breakwater design to reduce the footprint and minimize the negative consequences of reflected wave energy.

1.3.3. Increasing Floating Breakwater Effectiveness

Previous studies have aimed to reduce the size of a floating breakwater while increasing the effectiveness. In order to keep the designs simple, small changes to common designs have been investigated. For example, Pena et al. (2011) added fins to regular pontoon breakwaters as well as making a catamaran by attaching two pontoons together. Yan (2015) optimized a box breakwater by adding cantilevers at different locations on the box. He et al (2012) added pneumatic chambers to a floating box breakwater to increase the performance. Ji et al (2016) tested a model with a hollow rubber float topped with a mesh cage. Adding slotted barriers was found to reduce transmission and pitch response in smaller period waves (Huang, He, & Zhang, 2014).

While some of these breakwaters showed promising results, they still largely employed reflection as the primary attenuation mechanism.

There have been previous studies that aim to increase wave attenuation via alternative attenuation mechanisms. Ji et al (2015) tested a cylindrical floating breakwater which consisted of two cylindrical floats with a mesh cage suspended between them. The mesh cage was filled with hollow rubber balls that transferred the wave energy into mechanical energy. Alternatively, adding three to five skirt walls to the keel of a box breakwater was found to reduce the effective width by half (Neelamani & Ljubic, 2018). Twin pontoon breakwaters have also been modified using nets with sinkers attached to the keel, which decreased the transmission coefficient as the number of nets increased (Ji, Cheng, Yang, & Oleg, 2017). Mani (1991) tested a Y-Frame floating breakwater, which consisted of a trapezoidal float and a row of closely spaced large cylinders attached to the keel. This design produced a transmission coefficient of 0.5 with a width to wavelength ratio of less than 0.2. Pontoon breakwaters have also been modified with wing plates and a porous material attached to the sides, which reduced incoming wave energy by as much as 80% (Christensen, Bingham, Friis, Larsen, & Jensen, 2018). Wang and Sun (2010) also investigated porosity with a breakwater made of diamond shaped blocks. While these studies showed that the width to wavelength ratio can be reduced using alternative attenuation mechanisms, many of them still rely primarily on reflection. In addition, the material used in the model designs are not intended for full scale, long term field deployments. An investigation into alternative materials that produce a lighter, more easily deployable breakwater has yet to be conducted.

1.4. Conceptual Look at Turbulence

Turbulence can tentatively be thought of as violent unsteady motion comprised of many 3D eddies. Turbulence is closely related to the Reynolds number ($Re = uL_c/\nu$), which is the ratio of inertial to viscous forces, where u is the upstream flow velocity, L_c is the characteristic length, and ν is the kinematic viscosity. As the inertial forces increases above the viscous forces, flow disturbances emerge. The dependence on Re is classically demonstrated by flow around a cylinder (Figure 4).

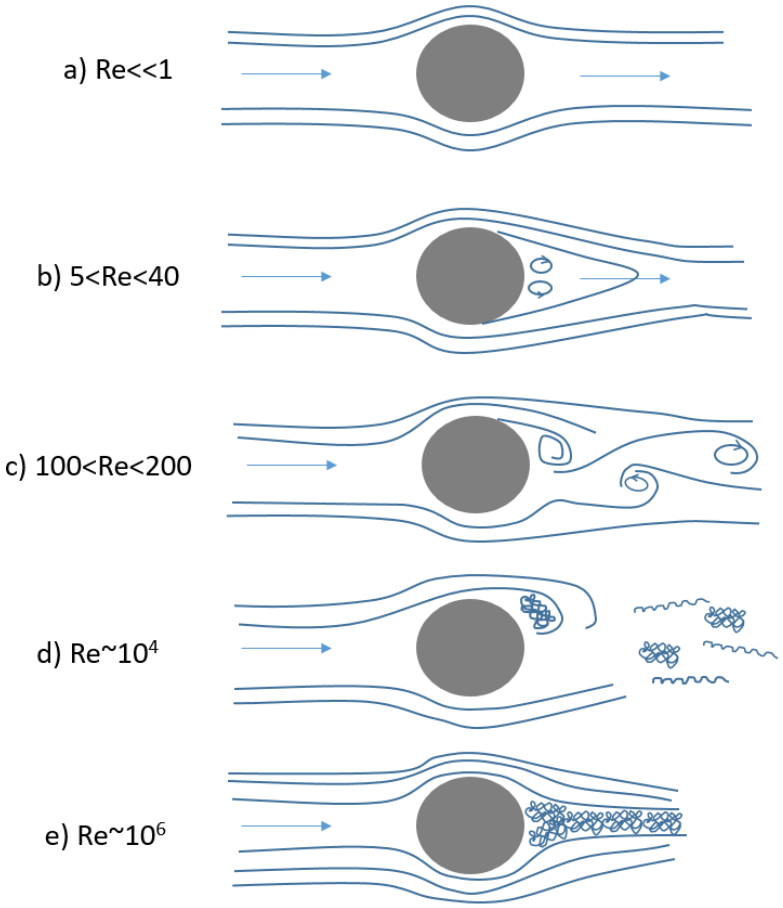

Figure 4. Flow around a cylinder based on Reynolds number. Flow is left to right around the cylinder (grey). Adapted from Turbulence: An Introduction for Scientists and Engineers (Davidson, 2015).

When viscous forces dominate (ie. Re<1 in Figure 1a) the flow is laminar with no formation of vortices (Davidson, 2015). The viscous forces maintain the same flow

before and after the cylinder. According to Davidson (2015), when the inertial forces start to dominate, 5 to 40 times the viscous forces, vortices begin to form behind the cylinder (Figure 4b). These vortices are stable and remain attached to the rear of the cylinder. Inertial forces 100 to 200 times greater than the viscous forces cause the vortices to peel off the cylinder (Figure 4c) and the formation of three-dimensional instabilities (Davidson, 2015). This continues to happen in a periodic manner. Once the Reynolds number reaches 10^4 the vortex shedding causes areas of turbulence form behind the cylinder (Figure 4d). When the Reynolds number reaches 10^6 a fully developed turbulent wake (Figure 4e) has formed behind the cylinder (Davidson, 2015).

The process that turbulence dissipates energy is by transferring energy from larger eddies to smaller vortices as they break up (Figure 5).

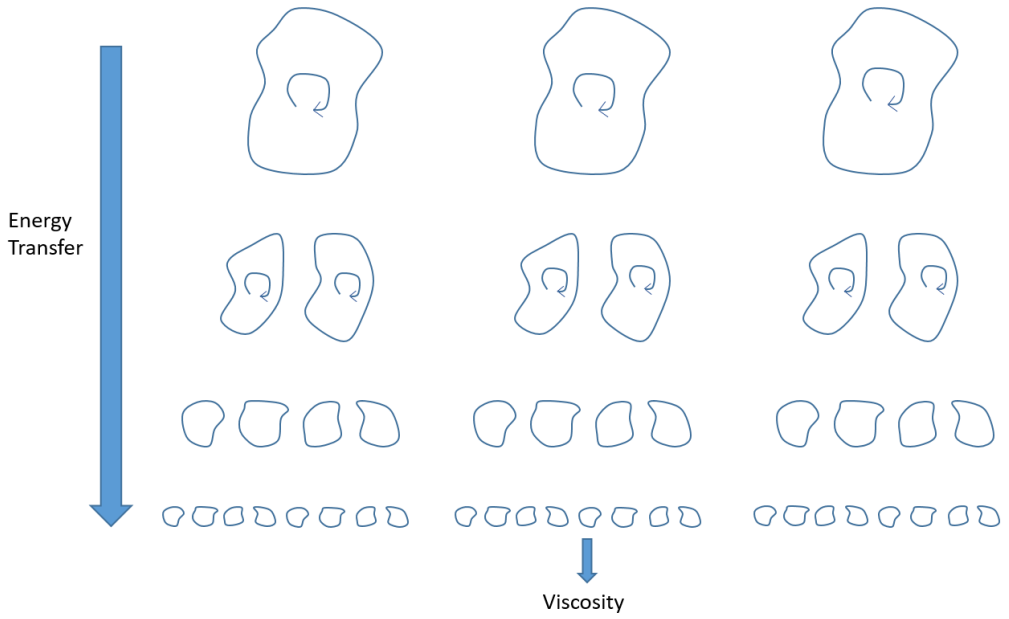

Figure 5. Evolution of energy transfer starting with larger eddies passing on energy as they break into smaller eddies eventually being absorbed by the viscosity. Adapted from Turbulence: An Introduction for Scientists and Engineers (Davidson, 2015).

Larger eddies will continue to break up into smaller and smaller parts while inertial forces dominate. As the size of the eddy decreases, the Reynolds number

decreases, as it is a function of the eddy size. Once the inertial and viscous forces equalize (Re~1) the process of breaking into smaller eddies stops and the viscosity absorbs the remaining energy.

In a wave field, assuming that the fluid is incompressible and follows Boussinesq flow, the flow can be separated into the sum of its components as

$$a = \bar{a} + \tilde{a} + a', \qquad [1]$$

where $\bar{a}$ is the time averaged component, $\tilde{a}$ is the wave induced periodic component, and a' is the turbulence component (Anis & Moum, 1995). The three different components also produce three components of energy, the mean kinetic energy (MKE), wave kinetic energy (WKE), and the turbulent kinetic energy (TKE).

Using a right-hand Cartesian system, the momentum equation for mean flow is

$$\frac{\partial \overline{U}_i}{\partial t} + \overline{U}_j \frac{\partial \overline{U}_i}{\partial x_j} = -\frac{1}{\rho}\frac{\partial \overline{P}}{\partial x_i} - \delta_{i3} g + \nu \frac{\partial^2 \overline{U}_i}{\partial x_j^2} - \frac{\partial}{\partial x_j}\left(\overline{u_j' u_i'}\right) - \frac{\partial}{\partial x_j}\left(\overline{\tilde{u}_j \tilde{u}_\iota}\right). \qquad [2]$$

Multiplying the momentum equation for the mean flow by the mean flow $(\overline{U})$ and averaging, the mean kinetic energy of the wave field is,

$$\frac{\partial}{\partial t}\left(\frac{1}{2}\overline{U U}\right) = \nu U \frac{\partial^2 \overline{U}}{\partial z^2} - \frac{\partial}{\partial z}\left(\overline{w' u' U}\right) + \overline{w' u'}\frac{\partial \overline{U}}{\partial z} \qquad [3]$$

Similarly, multiplying the wave and turbulent momentum equation by the periodic wave induced velocity $(\tilde{u})$ and averaging, the wave kinetic energy is,

$$\frac{\partial}{\partial t}\left(\frac{1}{2}\overline{\tilde{u}_\iota \tilde{u}_\iota}\right) = -u_i u_j \frac{\partial u_i'}{\partial x_j} - \frac{\partial}{\partial z}\left(\overline{w' \frac{1}{2}\tilde{u}_\iota \tilde{u}_\iota}\right) - \frac{\partial}{\partial z}\left(\overline{w' u_\iota' \tilde{u}_\iota}\right) + \overline{u_\iota' u_j' \frac{\partial \tilde{u}_\iota}{\partial x_j}} \qquad [4]$$

The turbulent kinetic energy is found by taking the wave and turbulent momentum equation and multiplying by the turbulent part of motion (u') and averaging;

$$\frac{\partial}{\partial t}\left(\frac{1}{2}\overline{u_i' u_i'}\right) = -\frac{\partial}{\partial z}\left[\overline{w'\left(\frac{p'}{\rho} + \frac{1}{2}u_i' u_i'\right)}\right] - \frac{g}{\rho}\overline{w'\rho'} - \overline{w'u'}\frac{\partial \bar{U}}{\partial z} - \frac{\partial}{\partial z}\left(\overline{w'\frac{1}{2}\tilde{u}_i \tilde{u}_i}\right)$$
$$-\frac{\partial}{\partial z}\left(\overline{\tilde{w}\frac{1}{2}u_i' u_i'}\right) - \overline{u_i' u_j'}\frac{\partial \tilde{u}_i}{\partial x_j} - \varepsilon \qquad [5]$$

The goal is to transfer energy from the WKE to the TKE. The last term in the WKE equation and the second to last term (production term) in the TKE equation are the same with the exception of the sign, implying this term is a sink in WKE and a source in TKE. It is through this term that energy will be transferred from the wave field to turbulence. When multiplied by the density, the term $u_i' u_j'$ is also known as the Reynolds stress term. In this research, the goal is to influence the Reynolds stress term by increasing turbulent velocities (u') in the system. This will be achieved through two approaches: wave breaking and vortex shedding. When depth-limited wave breaking occurs, turbulent motions are injected into the water column (Figure 6).

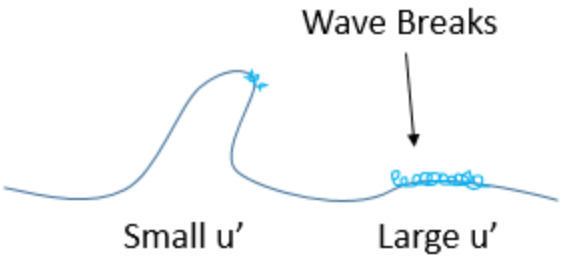

Figure 6. Breaking wave in a wave field moving left to right.

The increased turbulent motions (u') lead to increased Reynolds stresses, therefore wave breaking is one of the mechanisms being investigated.

The vortex shedding to increase Reynolds stresses, is another mechanism that will be investigated. Vortex shedding is an oscillation of vortices in the wake of a cylinder, which creates instabilities in the velocity profile. These instabilities are laminar close to the cylinder and transition to turbulence further away from the cylinder (Figure 7).

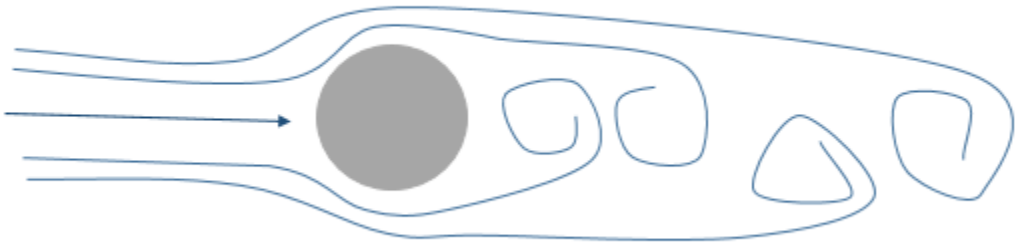

Figure 7. Vortex shedding induced by a cylinder (grey) inserted into a wave field. As shown water particles moving left to right, which would be under the crest of a wave. In trough, the vortex shedding would be the opposite, right to left.

The greater the vortex shedding, the greater increase in Reynolds stresses. In order to maximize the vortex shedding process, the diameter of the cylinder can be tuned using the Strouhal Number (St) with the desired wave environments. The Strouhal number is a

function of the Reynolds number (Re). Rearranging the vortex shedding frequency to solve for the required diameter,

$$D_{ia} = St\frac{u}{f_s}\,, \qquad [6]$$

where u is the maximum along channel fluid velocity, and f_s is frequency of the wave environment (Det Norske Veritas, 2010).

CHAPTER 2

METHODS USED IN DESIGN

2.1. Target Environment

The goal of this thesis is to create floating breakwaters that will yield a transmission coefficient of 0.5 in the target Sea State of 3 (SS3), which was selected due to the frequency it is observed in coastal applications. SS3 includes significant wave heights of 0.9 – 1.5 m and peak periods of 3 – 6 s (Briggs, 2001). In addition to achieving the reduction in energy, the structures must be designed to be practical. This includes being easily deployable, of manageable size for current ship infrastructure, and feature simplistic mooring lines.

2.2. Preliminary Design Work

All design work was conducted at full scale so that full-scale floating breakwaters could be deployed in the future. A review of existing design and laboratory testing practices informed the test campaign. A common design found in literature is the simple box breakwater; therefore, this design was used to validate existing design and testing practices. Using the desired environmental conditions and the simple shape, existing work could determine the nominal dimensions required. The width (dimension in the direction of the wave field) was determined using experimental data from Hales (Figure 8).

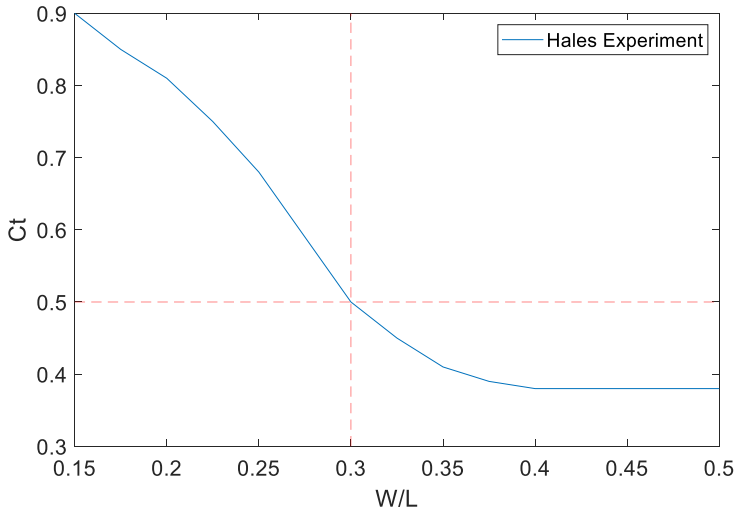

Figure 8. Floating box breakwater C_t versus W/L (blue line) data plotted from Hales Experiment (1981). Horizontal dashed line is target C_t of 0.5, vertical line shows the corresponding W/L ratio.

The width to wavelength ratio was 0.3 (Figure 8) based on the design C_t of 0.5. The longest wavelength of SS3 (with T=6 s) was 56.2 m at an operational depth of 20 m. A design width of 16.9 m along the direction of wave propagation was determined by multiplying the wavelength (56.2 m) by the W/L ratio (0.3).

The height of the box was determined by first finding the required draft. The draft was selected using the design curves based on the Macagno Theory (PIANC, 1994). This is a method for determining the transmission coefficient given a structure's width and draft. The structure must be rigidly moored (e.g. with piles) for the Macagno Theory, making its usage an estimate in this design, which is not rigidly moored. The following equation generated the design curves:

$$C_t = \frac{1}{\sqrt{1 + \left[\frac{\pi W \sinh\left(2\pi \frac{d}{L}\right)}{L \cosh\left(2\pi \frac{(d-D)}{L}\right)}\right]^2}} \quad [7]$$

where W is the breakwater width, D is the breakwater draft, d is the water depth, and L is the wavelength (Headland, 1995). The design curves are available for three L/d ratios: L/d=1.25, 2.5, & 5. The curves for L/d = 5 was chosen because the L/d was 2.8, which would yield a conservative draft. The design Ct of 0.5 at the W/L of 0.3 was used to determine the draft to depth (D/d) ratio of 0.4 (Figure 9).

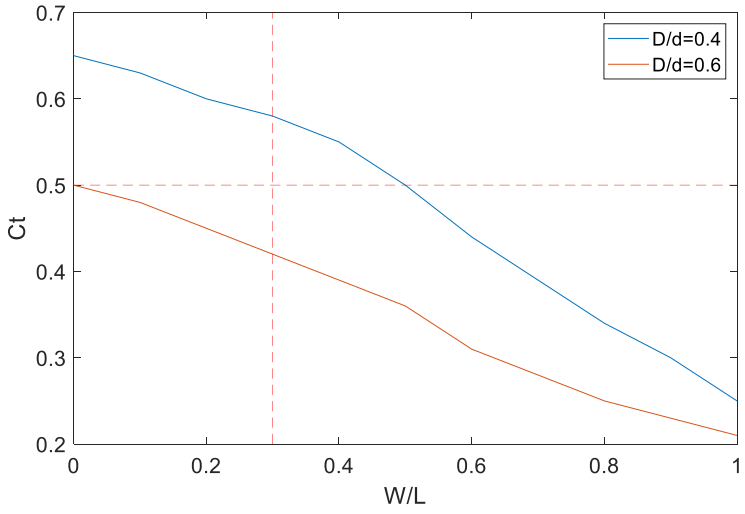

Figure 9. Ct versus W/L using Macagno Theory (PIANC, 1994). Blue line is D/d of 0.4 and the red line is D/d of 0.6. Horizontal dashed line at Ct goal of 0.5 and vertical dashed line at W/L of 0.3.

The draft was required to be at least 8 m for the target depth of 20 m. To ensure that the floating breakwater would survive more aggressive wave environments, a survival case with a wave height of 3.6 m was included. Therefore, in an effort to reduce the chance of overtopping, an additional 4 m of freeboard were added to the height of the breakwater for a total of 12 m.

The length, which is perpendicular to the wave direction, does not affect the performance of the breakwater other than the size of the protected area in lee of the structure due to diffraction. The required length was 40 m to keep the aspect ratio of the length to width close to 2:1. The scope of this research did not include determining the amount of protected area in lee of the breakwaters.

A hydrostatic analysis using the breakwater dimensions determined the center of gravity (COG), center of buoyancy (COB), moments of inertia, and the final draft. The COG was calculated using Equation 1;

$$COG = \frac{\sum_1^i m_i CG_i}{m_{tot}} \quad [8]$$

where i is the number of sections the structure is broken up into, m_i is the mass of the section, CG_i is the center of gravity of the section from the keel, and m_{tot} is the total mass of the structure. The COB was calculated by Equation 2;

$$COB = \frac{\sum_1^i V_i CB_i}{V_{tot}} \quad [9]$$

Where V_i is the submerged volume of the section, CB_i is the center of buoyancy of the section from the keel, and V_{tot} is the total submerged volume of the structure.

The initial material selection for construction of the breakwater was concrete due to its cost effectiveness and availability. The box breakwater was designed with 1 ft thick concrete walls.

2.2.1. ANSYS Aqwa Modeling

The box breakwater required performance validation prior to model construction, which was conducted in ANSYS Aqwa. ANSYS Aqwa is a finite element analysis program that uses potential flow theory and contains a toolset to investigate loads and motion responses to floating or fixed structures in various environmental conditions. Motion responses, mooring forces, and an estimate of the transmission coefficients in lee of the structure were determined with Aqwa.

Aqwa imported the design from SolidWorks and a finite element mesh was created (Figure 10).

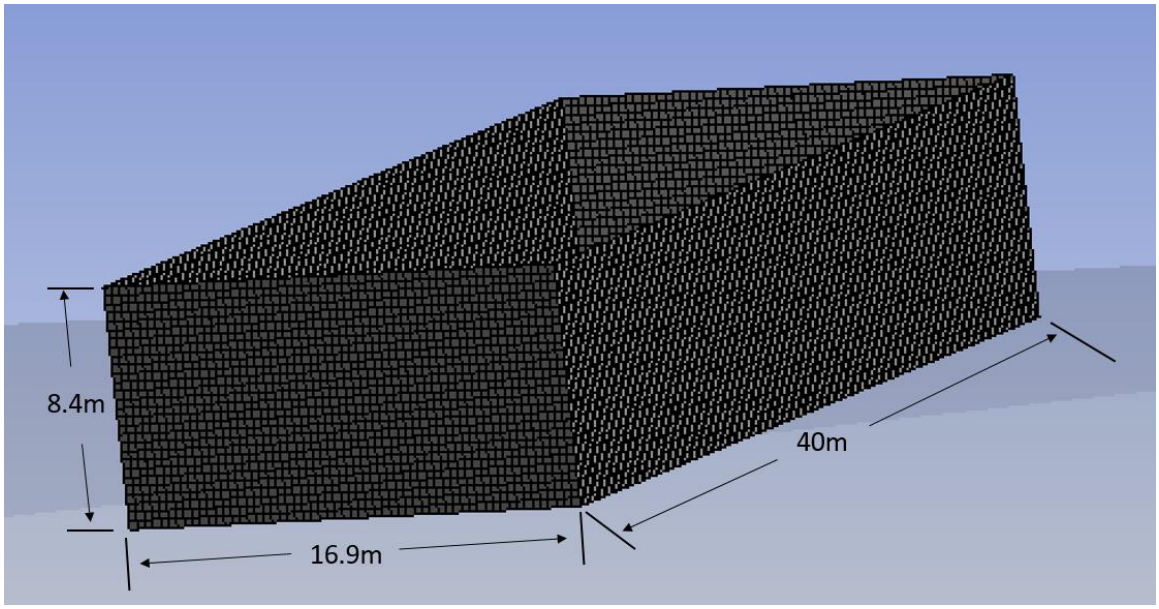

Figure 10. Box breakwater with finite element mesh in ANSYS Aqwa. The wave direction is right to left and the height of 8.4m is at the water line, Aqwa only uses sub-surface parts of the structure for analysis. The dimensions are the full scale.

The mesh consisted of 18,334 elements and 18,526 nodes with a maximum element size of 0.5 m. The four mooring lines were 180 m long catenary mooring lines weighing 92 kg/m and stiffness of 441,600 kN, attached to fixed anchor points. The time

domain response had a time step of 0.1 s and ran for 180 s. Test cases included regular waves using Airy Wave Theory (linear wave theory) for periods of 3, 4, 5, 6, 7,9, and 12 s and wave heights of 1, 1.5, and 2.75 m.

The results of ANSYS model for an incident wave height of 1.5 m and a period of 5 s resulted in a wave height of only 0.3m which is a Ct of 0.2 (Figure 11).

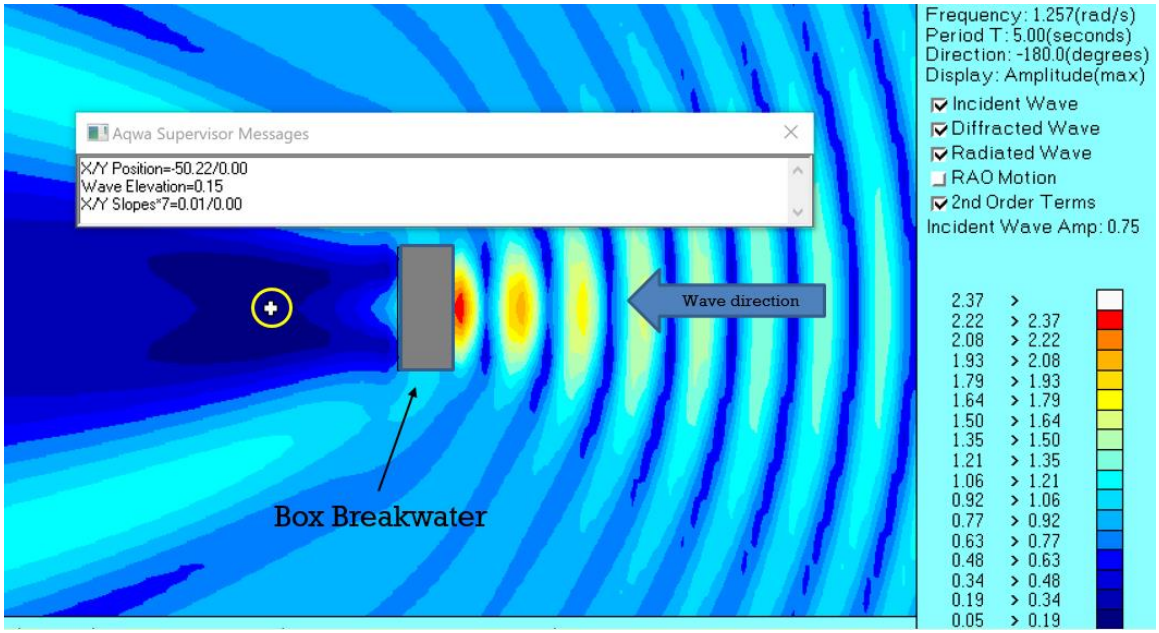

Figure 11. Snapshot from ANSYS Aqwa for box breakwater (grey rectangle). Regular wave direction from right to left with an incident wave height of 1.5m and a period of 5s. Wave height measurement of 0.3m taken at the crosshair in the yellow circle, which was 50m in the lee of the structure. The contours represent the amplitude of the waves, values can be seen in the colorbar to the right.

The Ct of 0.2 from the Aqwa analysis showed that the initial design should perform as predicted and attenuate SS3 in lee of the breakwater below the 0.5 goal. With a regular incident wave, the simulation depicts standing waves that form in front of the breakwater, indicated by yellow and red areas (Figure 11). One of the limitations of this analysis is that it uses potential flow, meaning the program ignores viscous effects. The wave height pattern in lee of the breakwater displays this. With diffraction around the

breakwater, the wave height pattern should converge as opposed to continuing to diverge. Even with this limitation, the design is successful due to the Ct of less than 0.5 in lee of the breakwater and advanced to the next phase.

2.2.2. Design Method Validation

Next, the preliminary box breakwater was evaluated with scaled model testing. The chosen Froude scale factor of 1:25 lies between the recommended ranges of 1:6 to 1:27 (Hudson, et al., 1979). The test setup consisted of 11 wave probes (Figure 12).

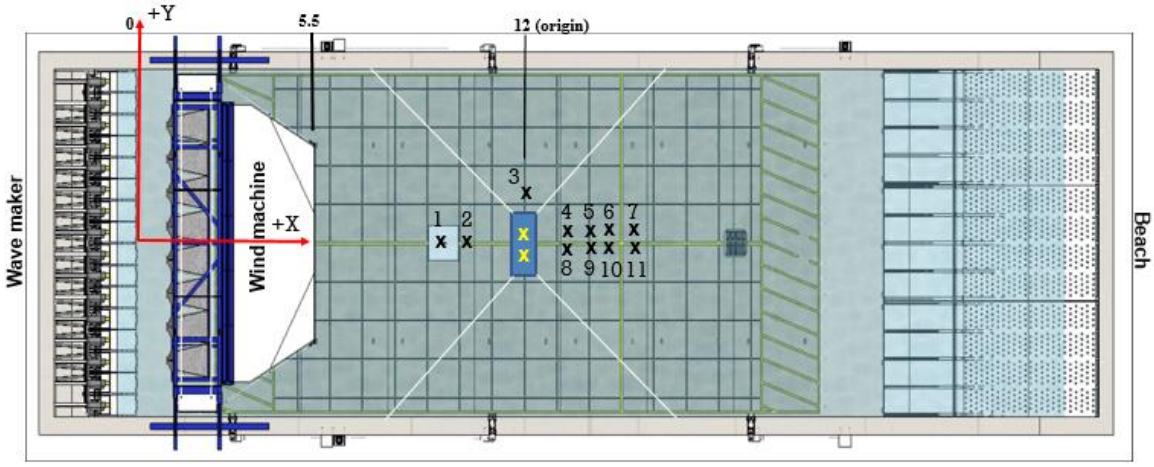

Figure 12. Experimental setup for preliminary box breakwater. The location of the breakwater is represented by the blue box and the mooring lines are the white lines. The locations of the wave probes are represented by x's. The yellow x's mark the location of calibration probes that were removed when the breakwater was installed.

The waves propagated from left to right, ending at the energy dissipating beach.

The box model was constructed of a 9.5 mm thick chemical-resistant pvc, which was chosen for its ease of cutting, ability to be plastic welded, and resistance to water absorption. To get the proper-scaled mass of 372.4 kg and to get the center of gravity in the proper location according to the hydrostatic worksheet, a layer of concrete was included inside the pvc shell (Figure 13).

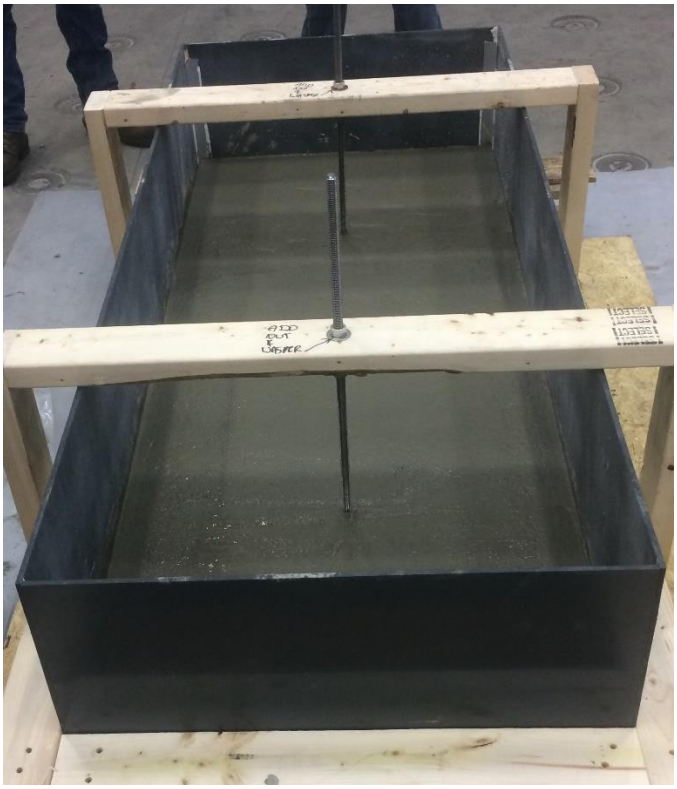

Figure 13. Box breakwater during construction, concrete layer poured. Wooden framework to keep it square and support the threaded rods that would function as lifting points.

The remainder of the space inside the pvc shell was filled with foam to reduce the amount of water that could penetrate the structure in the event of a leak. The finished model was 1.600 m long, by 0.676 m wide, by 0.476 m tall (Figure 14).

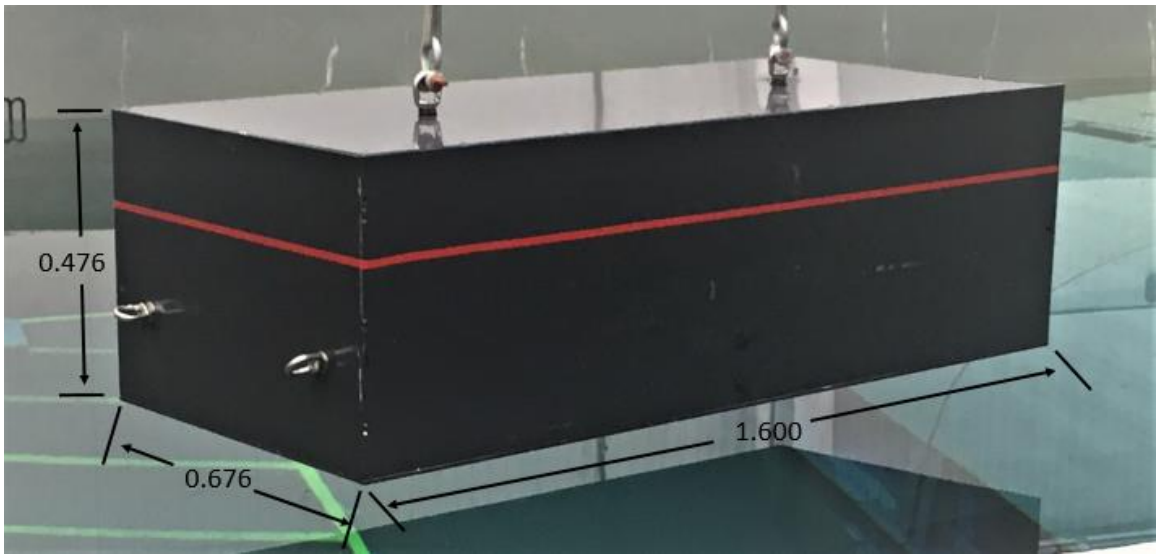

Figure 14. Completed box breakwater model weighing 372.4 kg. The red tape marks the waterline and the connections on the end are for the mooring lines. Dimensions in meters.

The box tested at a full-scale wave height of 1 m with periods ranging from 3 – 10 s. The Ct was calculated and compared to the width to wavelength (W/L) ratio in order to compare the experimental results to the design methods (Figure 15).

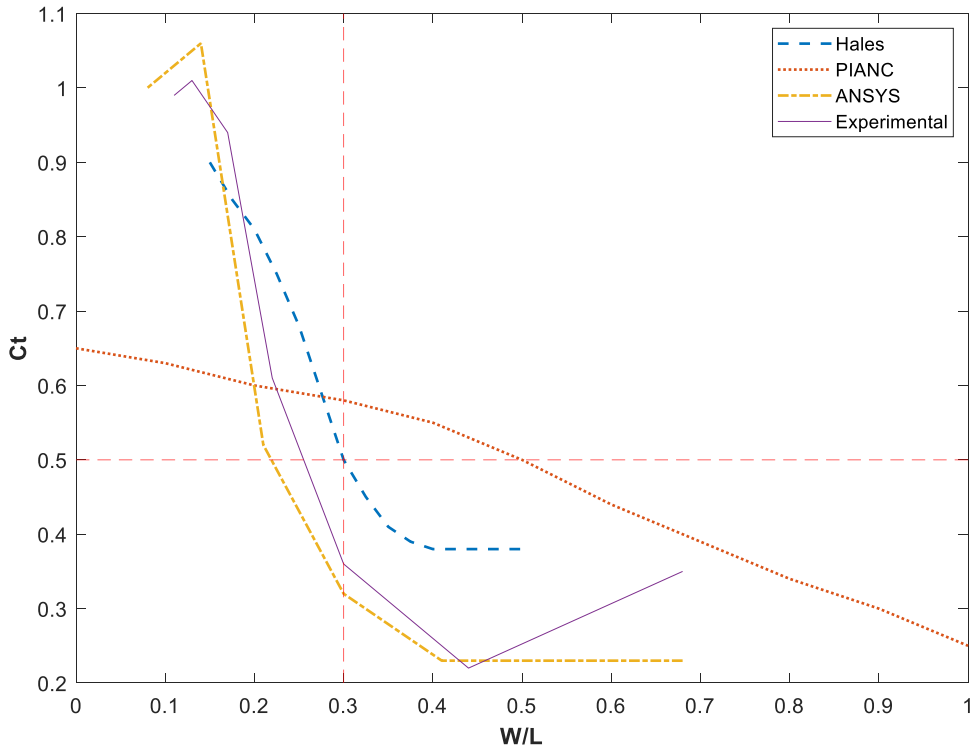

Figure 15. Comparison of wave height 1 m Experimental values (violet) to the design values from PIANC (dotted) and Hales (blue dashed) as well as ANSYS (yellow dot-dashed). The red dashed lines represent the results from the design criteria of a Ct of 0.5 and a W/L of 0.3.

The C_t values were calculated using the average wave height from the probes four through seven. The Aqwa wave height values were taken as an average of the values at the same locations as the 4 probes that were used to ensure the results would be comparable. The Ct vs W/L experimental and Aqwa results compared well with the design methods (Figure 15, violet and yellow dot-dashed respectively). The design achieved a transmission coefficient of 0.5 at a width to wavelength of slightly better than 0.3 (Figure 15). Despite ANSYS's limitations in taking into account frictional effects, the same trend was predicted as compared to the experimental results (yellow dot-dashed vs violet line Figure 15), which is largely due to the box utilizing reflection as its primary attenuation mechanism.

2.2.3. Review of Design Methods

The results from the preliminary test campaign validated the design process for future designs by achieving the desired C_t of 0.5 or lower for a W/L of 0.3. However, some aspects of the experimental campaign did not perform as expected. The reflection generated by the regular wave cases was problematic in the basin. A series of standing waves formed across the basin (+/- y direction). The basin was unable to settle without aid for many of the wave cases, as the settling time of 10 minutes was not adequate for these waves to diminish. Large foam blocks had to be inserted to interrupt the resonant behavior by damping the waves. In addition, the overall size and weight of the structure (over 1,500 metric tons) rendered the design unrealistic for real-world applications. With the design methods validated, the materials and the attenuation mechanisms employed was re-evaluated. The scale was reduced to 1:40 for the next round of testing in order to reduce the amount of reflection in the basin.

2.3. New Designs

Three new breakwater concepts comprised of various composite sandwich materials were designed at full scale. The use of composite sandwich material for a marine application was adapted from the previous design and testing of a composite hull special operations boat, MAKO, at the Advanced Structures and Composites Center. The first design, referred to as the box, is considered the baseline and primarily employs wave reflection as its wave attenuation mechanism. The second design, called the pipe model, utilizes vortex shedding, drag and reflection for wave attenuation. The third design is called the beach breakwater and uses wave breaking and reflection to attenuate wave energy. Composite materials make the breakwaters easier to transport and deploy while

reducing the overall weight. In fact, the designs made of the composite sandwich material weigh less than 10% of the same designs if they were made of concrete. The second and third designs are intended to determine if similar wave attenuation capacity was possible with half the footprint of the baseline design. Using a design that primarily utilizes reflection as a baseline to compare the effectiveness of alternative wave attenuation mechanisms is a practice that many other studies have employed (He et al 2012, Ji et al 2015, Yan 2015, Ji et al 2018).

2.3.1. Full Scale Box Design

The reflection based design used the validated design methods from the preliminary analysis to construct the overall dimensions is the box. The walls of the box were a 20.3 cm thick composite sandwich material consisting of 0.635 cm thick composite shell and 19 cm thick foam. The foam had a density of 80.09 kg/m^3 and the composite shell had a density of 1762 kg/m^3. The total mass of the structure was 200.8 metric tons. A water ballast, added to the interior of the box to drop to the desired draft, weighed 5,636 metric tons. The draft at the total weight of over 5.8 million kg, was 8.42 m which left a freeboard of 3.58 m. The COG was 4.4 m above the keel.

The full-scale width of the box was 16.9m, with a height of 12.1 m, and a length of 40 m. The calculated heave stiffness was 6.80 x 10^6 N/m, the pitch stiffness was 8.93 x 10^8 Nm/rad and the roll stiffness was 1.49 x 10^8 Nm/rad using the same equations and methods as the original box.

2.3.2. Full Scale Pipe Design

The second model, employing vortex shedding, drag, and reflection is the pipe design. It consisted of an inverted trapezoid with pipes attached to the keel, inspired by

the model in Mani (1991). The Re for this design was $1.3*10^5$ to $3.3*10^5$ which resulted in a Strouhal number of 0.21. This resulted in a full-scale diameter of 0.32 m. The pipes were 1.3 cm thick composite material and were designed hollow, thus filled with water. To have a footprint half the size of the box, the width of the top of the trapezoid was 8 m. The length was the same as the box (40 m). The bottom trapezoid width was 2 m and the trapezoid height was 5 m. The length of the pipes was 7 m. The pipe breakwater weighs 47.6 metric tons and requires a water ballast of 221.3 metric tons in the trapezoid. The COG was 8.32 m above the keel (bottom of the pipes), and the COB was 7.99 m above the keel. The calculated heave stiffness was 1.77×10^6 N/m, the pitch stiffness was 2.35×10^8 Nm/rad and the roll stiffness was 1.97×10^6 Nm/rad using the same equations and methods as the original box. The heave and pitch stiffness are 3-4 times smaller than the box and the roll stiffness is two orders of magnitude smaller.

2.3.3. Full Scale Beach Design

The third design utilizing wave breaking and reflection is the beach design. Once the waves break, the energy will dissipate as they move through the surf zone in the lee of the breakwater (Sorensen, 2006). For waves to set up and break, the beach had to remain in a semi-fixed position (limited movement in all degrees of freedom), therefore the mooring system had to be taut.

For the mooring system several types of nylon and polyester ropes were considered. This included Sampson ropes Eversteel-X, Amsteel Blue, RP-12 and the Bridon Ropes Superline Nylon and Superline Polyester. The stiffness (EA) was plotted against available rope diameters (Figure 16).

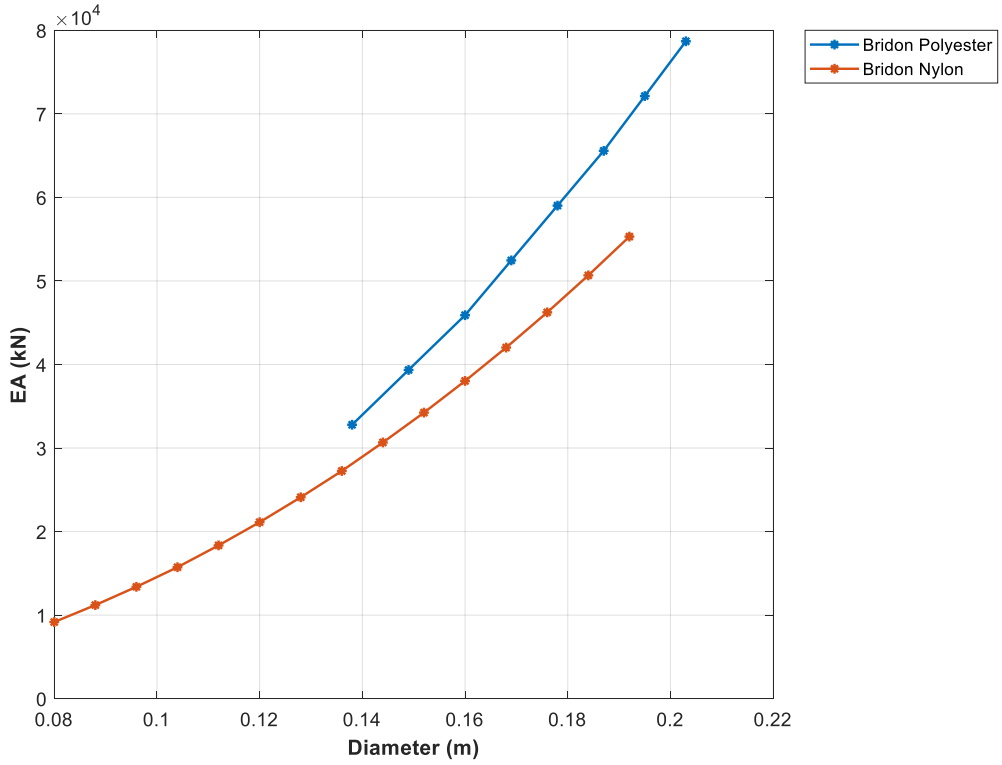

Figure 16.Bridon Polyester (blue) and Bridon Nylon (red) stiffness (EA) versus rope diameter.

The Bridon Polyester rope stiffness was close to a linear trend with increasing diameter, where the Nylon rope had a nonlinear stiffness. The estimated maximum force in the line was calculated using the maximum orbital displacements determined by linear wave theory, a period of 12 s and a wave height of 3.6 m. These environmental conditions are outside the normal use range. The estimated maximum line force in metric tons is then,

$$F_{max} = \sqrt{\left(\frac{EAdx}{L_R} cos^2\theta\right)^2 + \left(\frac{EAdy}{L_R} sin^2\theta\right)^2} \Big/ 10000 * FR_A \qquad [10]$$

Where, EA is the stiffness of the line, dx is the x-displacement of the wave orbital, dy is the y-displacement of the wave orbital, L_R is the length of the rope, θ is the angle between the sea floor and the rope, and FR_A is a force ratio from Aqwa. The force ratio was determined by taking the mooring line force from the concrete box Aqwa analysis and dividing it by the calculated estimate of force in the line for the original concrete box. The value of the ratio is 0.78, which was used to get a more accurate estimate of the mooring force. The Bridon Polyester Superline was the only rope that the breaking force exceeded the maximum estimated force with fewer than eight lines required. Six Bridon Polyester Superlines with a diameter of $6\ 5/8$ inches were selected for this design. The line is constructed of parallel laid polyester sub-ropes encased in a polyester jacket with an integrated particle filter system (Bridon-Bekaert Ropes Group, 2018).

The beach structure was designed to provide the required pretension with its own ballast. The total required buoyant force to restrict the natural period in heave under 3 seconds was 1,159 metric tons. This resulted in a required removable water ballast of 1,159 m^3. The mid and bottom braces as well as the front and back wall supports, were designed to be filled with water once the structure was in the desired operational location. This would drop the structure to be just below the operational draft. The mooring lines would then be connected and the ballast pumped back out of the structure. As the ballast is pumped out, an upward buoyant force will put the desired pretension on the mooring lines.

The beach width was 8.56 m, height 12 m, and length 40 m. The structure weighed 400.2 metric tons. The COG was located 3.77 m above the keel and the COB was 4.87 m above the keel. The calculated heave stiffness was 1.05 x 10^6 N/m, the pitch

stiffness was 1.34 x 10^8 Nm/rad and the roll stiffness was 1.13 x 10^7 Nm/rad using the same equations and methods as the original box. These calculations use the structure itself and do not include the ballast or mooring lines.

2.3.4. Testing Setup

The experiments were conducted at the Wind and Wave Basin (W2) in the Advanced Structures and Composites Center at the University of Maine. The W2 is 30 m long, 9 m wide, 4.5 m deep, with an energy-absorbing beach at one end and a 16 paddle wave maker at the other (Figure 17). The wave maker can generate regular and irregular directional wave conditions, with a maximum wave height of 0.8 m at a period of 2.3 seconds.

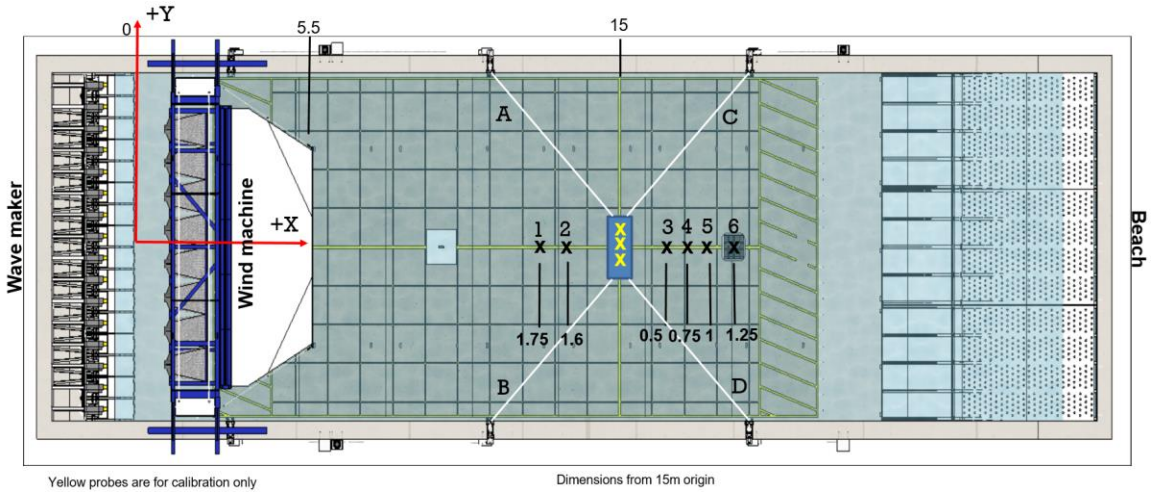

Figure 17. Plan view of the W2 basin with experimental set up. The basin coordinates origin is located in the middle of the front face of the wave maker shown with red arrows. The positive Z direction is up with zero at the mean water level. The beach is located on the right hand side and the wave maker on the left. Directly in front of the wave maker is the wind machine, which sits on the basin wall above the water surface (not used in this experiment). The light blue box represents the location of the breakwaters. Wave probe locations are marked with an "x". Wave probe distances are from the center of the basin (15, 0, 0) and are in meters. The yellow "x" wave probe locations were used in calibration runs only. White lines are the primary mooring lines, labeled A-D.

The box and beach breakwaters both had 4 mooring lines (white lines Figure 17). The pipe model had 8 mooring lines, with 4 set up similar to the other breakwaters and

the additional 4 attached to the bottom stiffener plate. The purpose of the 4 mooring lines connected to the bottom were to keep the pipes oriented in a vertical manner. The mooring lines were all cables with springs to achieve the desired stiffness.

The mooring lines for model testing consisted of a ¼" diameter wet environment rope with a spring attached. Once installed each model had a different pretension in the lines. The pretension was to keep the mooring lines from going slack in the box and pipe breakwaters. The full-scale pretension for the box was 950.2 kN which was about double the pipe at 594.1 kN. The highest was the beach at 2,949.3 kN in pretension. This was the highest due to attempting to reduce the heave and surge natural periods that would help simulate a taut fixed mooring system.

2.3.5. Instrumentation and Wave Environments

Water surface elevations were recorded by six Akamina AWP-24-3 capacitance style probes with a 1 m long sensor element and output a ± 5 Vdc signal at a rate of 50 Hz. The four primary mooring lines were equipped with Interface load cells sampling at 50 Hz. Qualisys Motion Capture System recorded the motion response in 6 degrees of freedom for all models (Figure 18).

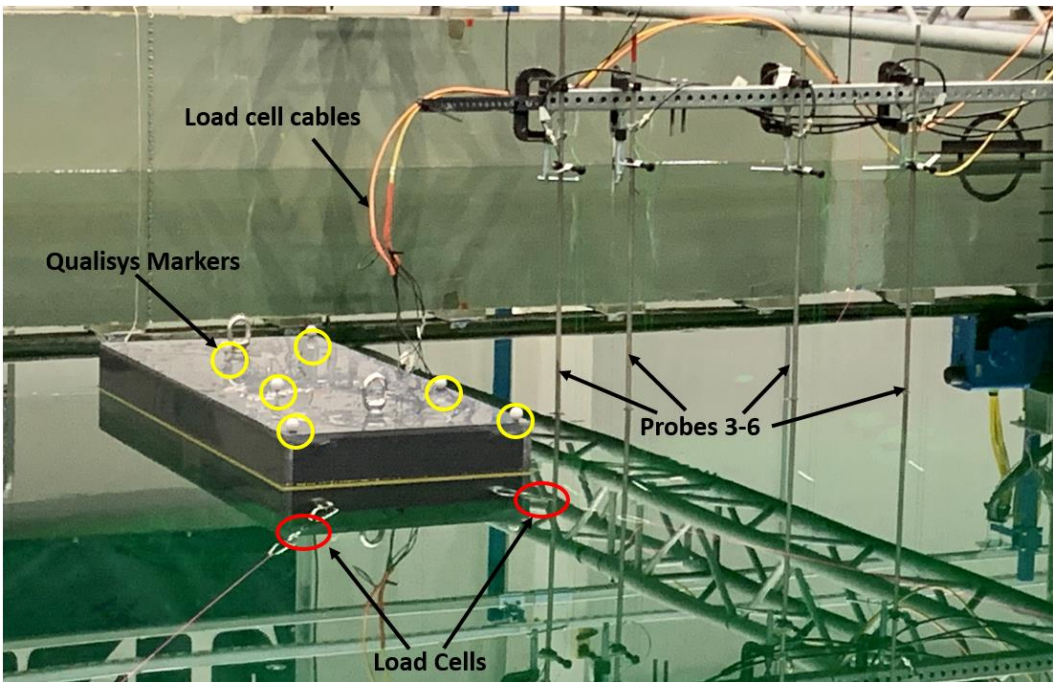

Figure 18. Box breakwater, with instrumentation, in basin and ready for testing. The four capacitance probes in lee of the breakwater (3-6), Qualisys markers in yellow circle, the port two load cell locations shown in the red circles.

The testing consisted of seventeen regular wave cases comprised of full-scale wave heights ranging from 1 - 2 m and periods ranging 3 - 8 s. Each wave case ran with and without the models. The cases without models are calibration cases that are also used for incident conditions. The selected wave environments resembled the preliminary test campaign. The environmental conditions were scaled at 1:40 according to Froude Scaling Principles (Table 1).

Table 1. Regular wave heights and periods tested, listed at model scale.

H (m)	T (s)
0.03	0.47, 0.63, 0.79, 0.95, 1.11, 1.26
0.04	0.47, 0.63, 0.79, 0.95, 1.11, 1.26
0.05	0.63, 0.79, 0.95, 1.11, 1.26

Froude scaling is commonly used in coastal and ocean scale model experiments. Froude scaling can be used when inertial forces dominate viscous effects. The Reynolds number is the ratio of inertial to viscous effects, and therefore it is commonly used to determine if Froude scaling can be used. For this research the Reynolds number for the full scale had a minimum value of 3.5×10^5, compared to the minimum of 1.2×10^3 for model scale. Both of these Reynolds numbers result in drag coefficients close to one, however they will be slightly different. It is important to investigate the Reynolds number for any scaled experiment. A limitation of any scale model testing is the possibility that viscous effects were captured during this testing.

2.3.6. Models

The outside of the box (Figure 19) was 9.5 mm thick chemical-resistant polyvinyl chloride (PVC) sheets, selected due to the ability to weld and form. Inside the pvc shell of the box was a 50.8 mm thick layer of concrete. The layer of concrete added mass and placed the center of gravity in the desired location referenced to the design. High-density foam filled the rest of the cavity to prevent the model from sinking in the event that the model leaked. The box model weighed 89.5 kg.

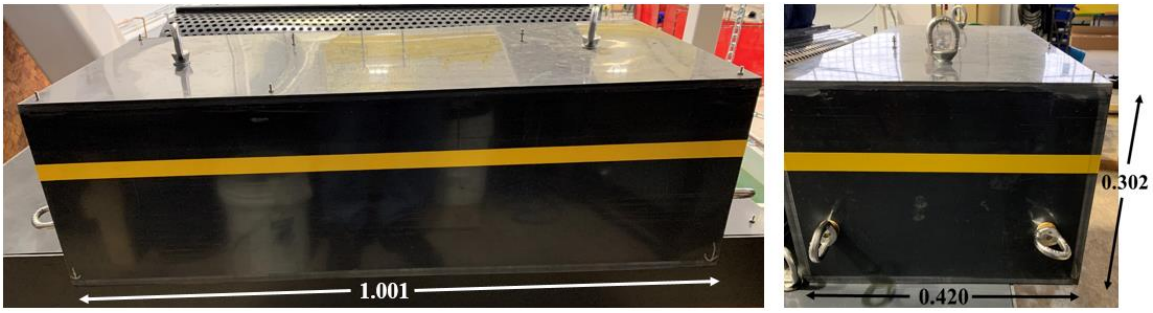

Figure 19. The left panel shows the windward side of the box model design. The right panel shows a profile view of the box with waves propagating from left to right. Eye hooks on sides are for mooring line connection and on the top for breakwater placement. The top of the yellow line is the design water line. Dimensions are model scale and in meters.

The pipe breakwater designed to attenuate wave energy through drag and reflection, weighed 4.74 kg (Figure 20).

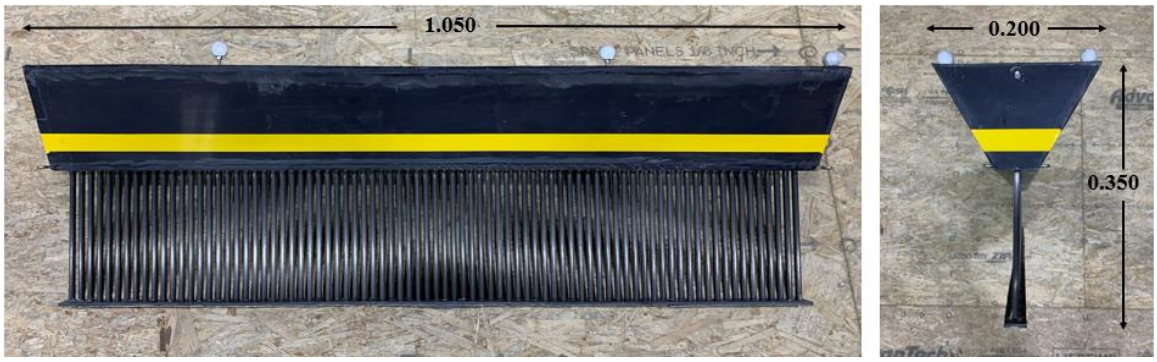

Figure 20. The windward side (left) of the pipe model design and the profile view (right) with waves propagating left to right. The top of the yellow line is the design water line. Dimensions are model scale and in meters.

The trapezoid was made of 3.2 mm thick chemical-resistant PVC and the pipes were pultruded carbon tubes with a diameter of 8 mm and a length of 175.3 mm. A 3.2 mm thick piece of PVC attached near the bottom of the pipes kept the pipes rigid in the oscillating wave field. The inside of the trapezoid was filled with foam to maintain buoyancy in the event the structure took on water.

The beach breakwater weighed 18.89 kg and was designed to attenuate through wave breaking induced turbulence and reflection, was the (Figure 21).

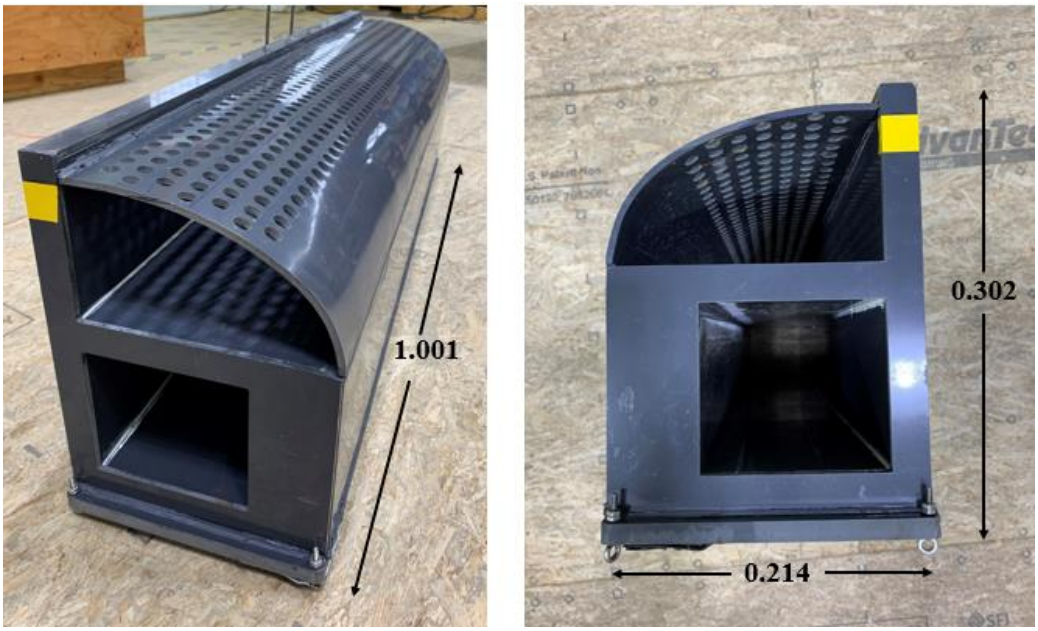

Figure 21. On the left is the beach model showing the length. On the right is a profile view with waves propagating left to right. The top of the yellow line is the designed water line. Dimensions are model scale and in meters.

The beach model was made of 9.5mm thick pvc. The holes have a 1.27 cm diameter and result in a 25% porosity on the upper section. This provided some additional attenuation and allowed breaking waves to drain.

The width for both the beach and pipe model is approximately 50% of the box width. While the lengths are all comparable, the beach and pipe model are half the footprint of the box. The beach model weighs 20% of the box and the pipe weighs only 5% of the box.

2.3.7. Data Processing

Even though the experiments were forced with a regular wave field, secondary waves were generated by the motion of the structure itself, wave reflection, basin sieching and through wave-wave interaction, which created a distribution of waves of various frequencies. Therefore, the total wave energy over the entire measurement period for each wave case was used to evalute the wave attenaution capacity. The energy was calculated by taking the variance of the power density spectrum (PSD) to determine the total energy per unit surface area:

$$E_{tot} = \frac{1}{2}\rho g\langle\eta^2\rangle \quad [11]$$

where ρ is the density of water, g is the acceleration due to gravity, and $\langle\eta^2\rangle$ is the variance (Chen & Belcher, 1999 & The SWAN team, 2006). The PSD was calculated using the following equation:

$$PSD = 2 * |fft|^2/L_f/df \quad [12]$$

where fft is the fast Fourier transform of the data, L_f is the length of the frequency spectrum, and df is the frequency step. Spectra were calculated in 50 second segments with 50 % overlap and a Hamming window (Figure 22). An average spectrum was analyzed for each 3.5 to 8.5 min experiment. The variance (η) can then be calculated as the area under the PSD curve or,

$$\eta = \int PSD. \quad [13]$$

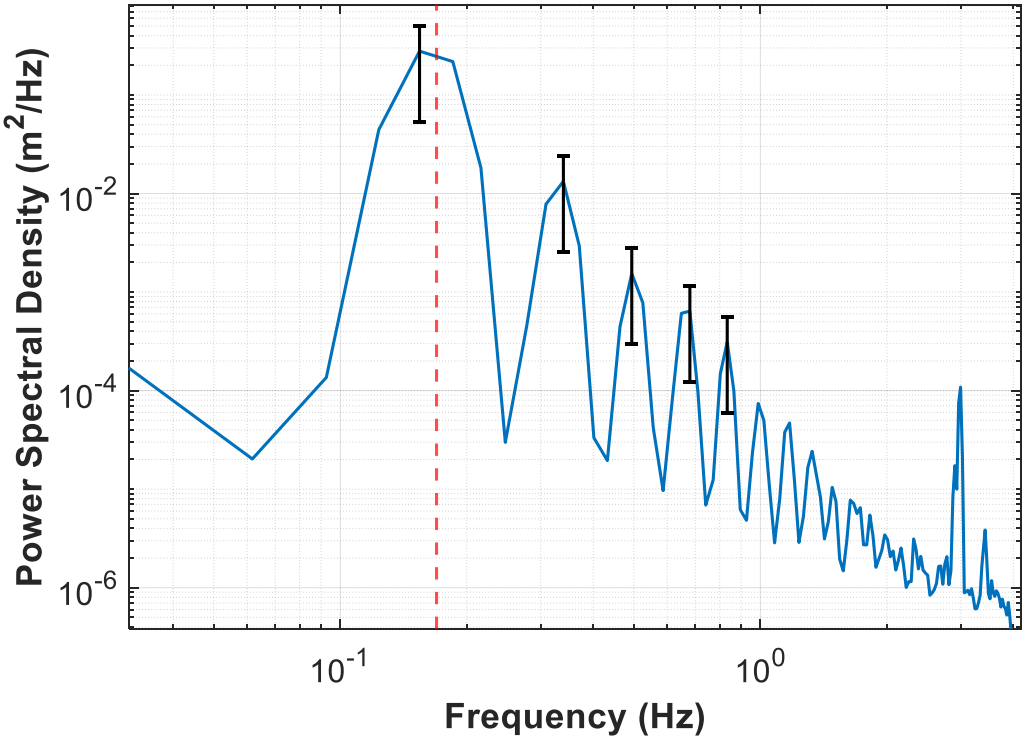

Figure 22. A loglog plot of the Power Density Spectrum vs frequency for a period of 5.9 s and wave height of 1.15 m full scale. This sample is an average transmitted PSD for the four wave probes in lee of the box breakwater during testing. The black bars represent 95% confidence intervals and the red dashed line is the incident wave frequency.

In Figure 22, the dominant energy is at a frequency of 0.1544 Hz, which corresponds to a period of 6.5 s. The peak is slightly shifted from the incident frequency due to the nonlinear effects introduced in lee of the breakwater from the breakwater motions and reflection off the basin walls. Several other peaks emerge in this sample PSD calculated from equation 12, which is why energy reduction of the distribution was waves was evaluated instead of the of dominant wave height.

The incident wave energy (E_i) was determined by averaging the PSD (determined from equation 12) recorded from the three calibration probes, integrating using equation 13 to get the variance, and then using the variance in equation 11. All three calibration probes were located in the position where the models would be stationed, and all test runs

were recorded in a calibration phase with no model present. The models took the place of the calibration probes once calibration runs were complete. For quality control purposes, only cases where the prescribed and observed wave heights were within 10% of each other were included in this analysis.

The reflection coefficient (Cr) is the reflected energy divided by the incident energy, E_r/E_i. The reflected energy is determined by first taking the maximum PSD value at each frequency between the two windward probes and then subtracting the incident PSD value for each corresponding frequency. The resulting PSD is integrated as shown in equation 13 to find the variance, which is used in equation 11 to determine the energy. Selecting the maximum PSD value for each frequency of the two windward probes minimized the impact of the reflected waves having different node and antinode locations for various models.

The transmission coefficient (C_t) is the transmitted energy divided by the incident energy, E_t/E_i. The transmitted energy is an average of the PSD values for each frequency recorded at each of the probes in the lee of the breakwater (probes 3-6). This averaged valued was then used to calculate the variance (equation 13), which was used to determine the energy (equation 11).

When no breakwater is present, the incident wave energy is equal to the transmitted wave energy. The presence of the breakwater introduces reflected wave energy and dissipated wave energy into that balance. The wave attenuation capacity of turbulence induced by the breakwaters is represented within the dissipated wave energy, E_d, calculated with the dissipated PSD values (PSD_d):

$$PSD_d = PSD_i - PSD_r - PSD_t, \quad [14]$$

where PSD_d is the power spectral density of the dissipated energy per frequency, PSD_i is the incident energy per frequency, PSD_r is the reflected energy per frequency, and PSD_t is the transmitted energy per frequency. The PSD_d was used to find the variance from equation 13 and then the dissipated energy (E_d) using equation 11. The term E_d is a remainder term, meaning that it could have contributions from mechanisms other than wave dissipation, such as form drag, energy created by the motion of the breakwater, energy losses from wave-wave interaction, etc. These subtractions were all done in spectral space. The dissipation coefficient (C_d) is the dissipated energy divided by the incident energy, E_d/E_i.

Confidence intervals were determined to help understand the statistical significance of the trends in the data. This was done by breaking the wave amplitude data into Hamming windowed segments. Each window contained 200 data points and they overlapped each other by 50%. The equivalent degrees of freedom for a Hamming window is $2.5164(N_{pts}/M)$, where N_{pts} is the number of data points in the time series and M is the half width of the window (Emery & Thompson, 2014). The degrees of freedom and the confidence interval (0.05-0.95 here) were used in a chi-squared (χ^2) table to determine the corresponding χ^2 values. The upper and lower bounds were then determined using;

$$CI_{lower} = \frac{(\nu-1)s^2(f)}{\chi^2_{1-\alpha}} \quad [15]$$

and

$$CI_{upper} = \frac{(\nu - 1)s^2(f)}{\chi^2_{\alpha}} \quad [16]$$

where ν is the degrees of freedom, $s^2(f)$ is the standard deviation of the frequency spectrum, χ^2 is the chi-squared value, and α is the desired confidence (0.05 here). To get the standard deviation, the PSD for each window segment was determined and integrated to get the variance per equation 13. The variance for each windowed segment was then used to calculate the energy per equation 11, resulting in an array of 27 energies at each probe location for each wave case. To determine the values in lee of the breakwaters (for transmission), the four probes in lee of the breakwaters were averaged, creating a 27 by 1 array of energies. To determine the values windward of the breakwater (for reflection), the maximum energy value recorded in the first two probes was used. The leeward values were divided by the incident values from the calibration runs. This resulted in an array of 27 transmission coefficients for each wave case. The standard deviation was taken on this array, and this was used in equations 15 and 16 to determine the upper and lower confidence intervals. The CI_{Lower} was then subtracted from the CI_{Upper} to form an array of errors. This error array was then plotted in Matlab using the errorbar function to add confidence intervals to the data. The process was repeated to obtain the reflection and dissipation confidence intervals.

CHAPTER 3

RESULTS

3.1. Transmission Coefficient

In order to evaluate how the wave attenuation capacity of each breakwater changes with wavelength, the transmission coefficient was compared across multiple wave periods at a given wave height. Due to similar trends in all three wave heights, only coefficients from the minimum (1.15 m) and maximum (2 m) wave height experiments are shown here (Figure 23 and Figure 24 respectively).

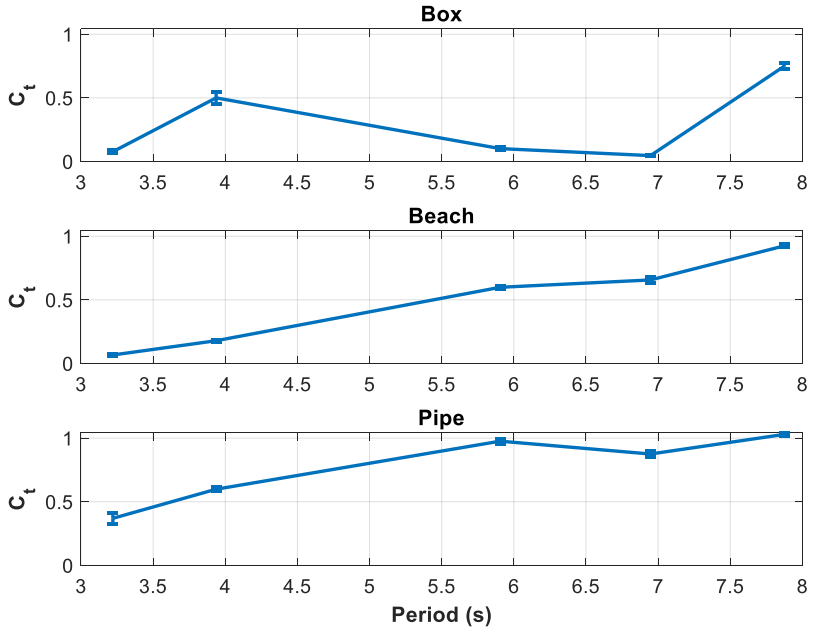

Figure 23. Transmission coefficient (C_t) versus period for the box (top), beach (middle), and pipe (bottom) breakwaters. Results shown in full scale for a wave height of 1.15 m. Vertical lines represent the 95% confidence intervals. Data at a period of 5 s omitted due to over 10% error in calibration.

The transmission coefficient, C_t, for an incident wave height of H_i= 1.15 m tended to increase with increasing wave period for the beach and pipe breakwaters, which indicated reduced wave attenuation with larger wave lengths. C_t associated with the box remained

below 0.5 for wave periods smaller than 7.5 s, which indicated that more than 50% of the wave energy is attenuated by the structure. The beach featured $C_t < 0.5$ for wave periods smaller than 5.5 s and $C_t < 0.5$ for the pipe breakwater for $T < 3.75$ s. Once $C_t = 1$ the breakwater is, in essence, riding the waves and the incident energy equals the transmitted energy.

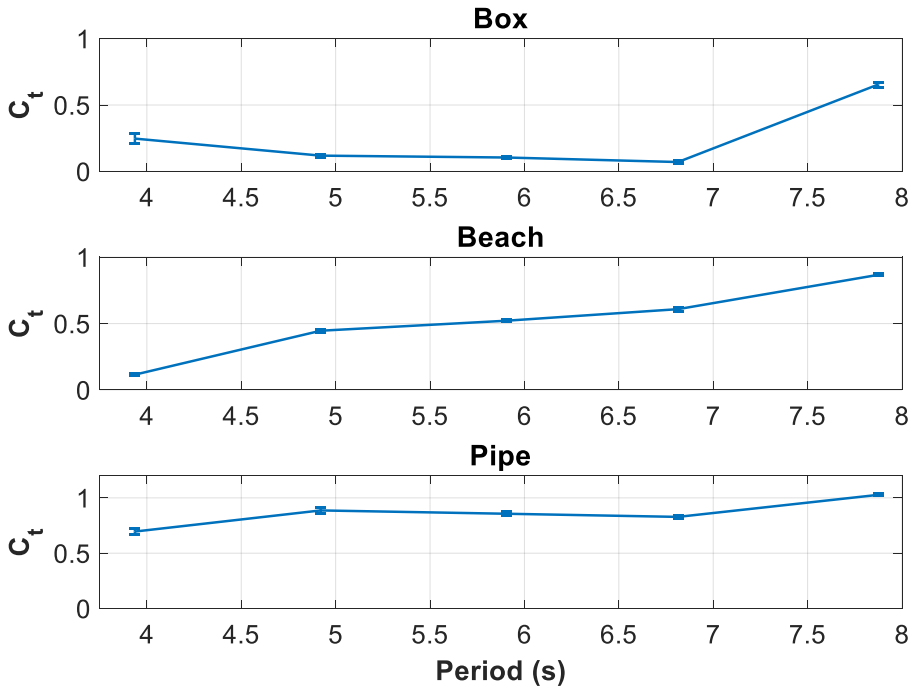

Figure 24. Transmission coefficient (C_t) versus period for box (top), beach (middle), and pipe (bottom) breakwaters. Results shown in full scale for a wave height of 2 m. Confidence intervals represented by vertical lines. Wave period around 3.5 s omitted due to calibration error greater than 10%.

Qualitatively, C_t trends were similar for $H_i = 2$ m compared to $H_i = 1.15$ m, where the wave attenuation capacity decreased for longer waves. The increased wave height had little effect on the box breakwater C_t, which remained below 0.5 until 7.5 s (Figure 24).The transmission coefficient for the beach breakwater reduced slightly by the increased wave height, remaining under 0.5 until a period of 5.25 s, which was a period 0.25 s shorter than the 1.15 m case. The pipe breakwater no longer has a transmission

coefficient below 0.5, meaning that it lost effectiveness with increased wave height, as it allowed 50% more energy.

3.2. Reflection Coefficient

The reflection coefficient (C_r) shows how much of the incident energy was reflected by the structure. A higher reflection coefficient coincides with more energy reflection by a given breakwater. A C_r of one signifies all incident wave energy was reflected and a value of zero signifies no reflection. The reflection coefficient versus period for the three breakwaters was plotted to compare the reflection potential for each structure (Figure 25).

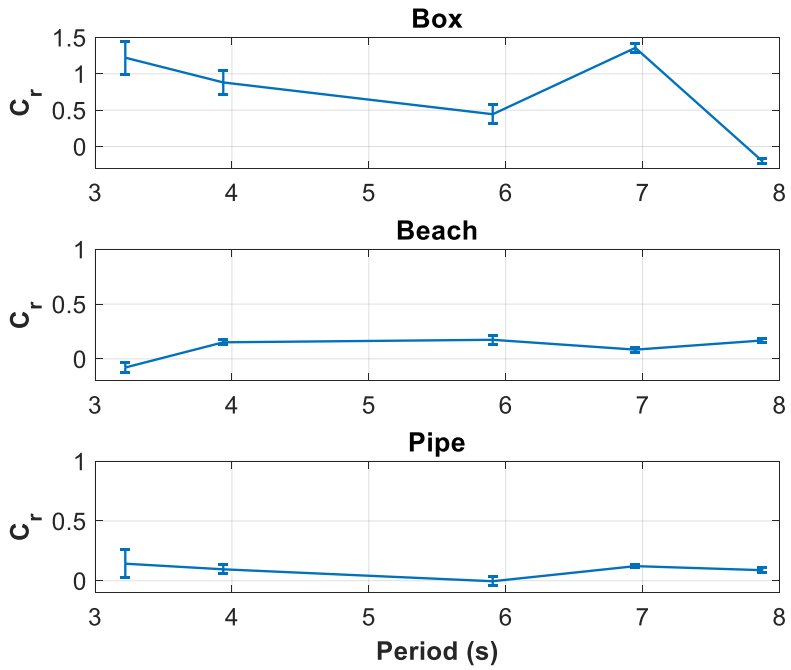

Figure 25. Reflection coefficient (C_r) versus period for the box (top), beach (middle), and pipe (bottom) breakwaters. Results shown in full scale for a wave height of 1.15 m. Confidence intervals represented by vertical lines. Data point at a period of 5 s omitted due to over 10% error in calibration.

The box breakwater had several values over one (top panel Figure 25), which should not be possible without external sources of energy. It was discovered that the

frequency in some of the wave cases was close to the natural frequencies of the basin and the box. This resulted in increased wave heights due to the resonant behavior, which is detailed in Appendix A. The box reflects most of the energy for the smaller wave periods, with a decreasing trend from 1.0 to 0.4 as the wave period increases from 3.2 to 5.9 s. The exception is around the period of 6.9 s, which is due to the frequency of the wave environment coinciding with the natural frequencies of the basin and the box. Once the period reached 7.8 s, the box no longer reflected any energy. The beach does not reflect any energy at the smallest period of 3.2 s, while it reached a peak C_r of 0.2 at a period of 3.9 s (middle panel Figure 25). The C_r decreased to 0.08 at a period of 6.9 s. The pipe breakwater's C_r never exceeded its peak of 0.14 at a period of 3.9 s. The beach and pipe breakwaters both had negligible reflection compared to the box.

The increased energy due to the 2 m wave height coupled with the resonant behavior of the box and basin, resulted in significant reflections in the basin during the box testing (Figure 26).

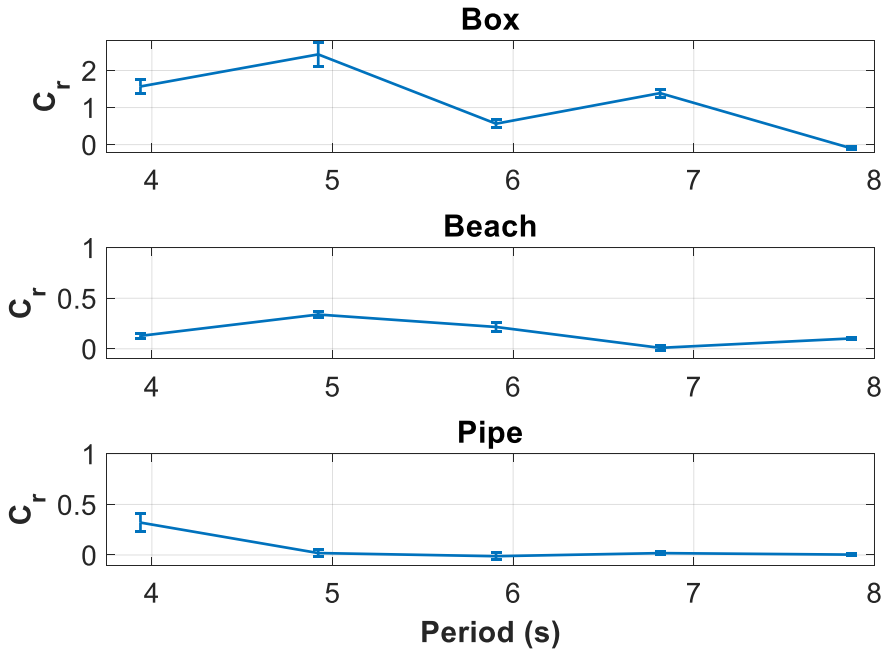

Figure 26. Reflection coefficient (C_r) versus period for the box (top), beach (middle), and pipe (bottom) breakwaters. Results shown in full scale for a wave height of 2 m. Confidence intervals represented by vertical lines.

The box reflection values for periods of 3.9, 4.9, and 6.8 s were above one (top panel Figure 26) and is explained in more detail in Appendix A. The C_r for the box again dropped to zero for the 7.8 s wave period. Due to these unrealistic reflection coefficient values for the box, the dissipation for a wave height of 2 m was not calculated. The beach breakwater increased from a C_r of 0.13 to 0.34 from periods 3.9 to 4.9 s, before dropping to zero at a period of 6.8 s (middle panel Figure 26). This peak (0.34) was 2.4 times greater than the peak of 0.14 for the 1.15 m wave case. The pipe breakwater C_r was 0.32 at a period of 3.9 s (bottom panel Figure 26). This was the highest period of reflection, as it dropped to zero at a period of 4.9 s and continued to produce no reflection for the remainder of the wave periods. This peak reflection (0.32) was 2.3 times greater than the peak (0.14) for the pipe breakwater with the 1.15 m wave height.

3.3. Dissipation Coefficient

In order to determine how much wave attenuation was attributed to dissipation rather than reflection, the dissipated energy was investigated. Values of C_d closer to one indicate greater energy dissipation, while a C_d near zero means no energy is attenuated through dissipation. The box breakwaters dissipation trends are near zero except for 5.9 and 7.9 s wave periods (top panel Figure 27).

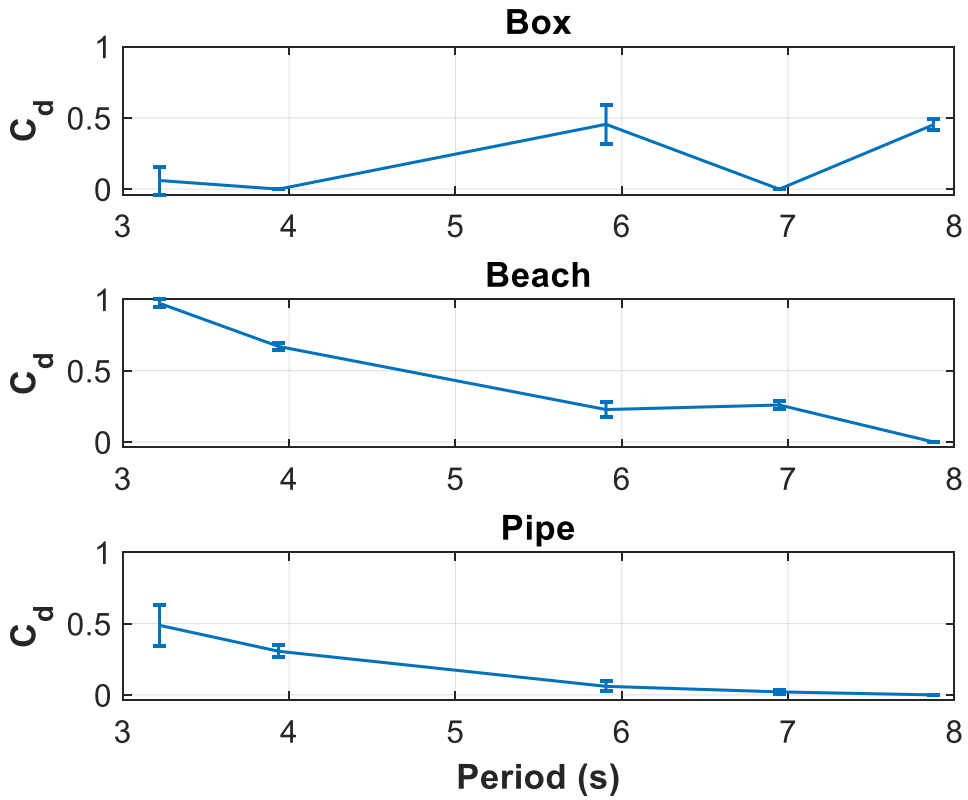

Figure 27. Dissipation coefficient (C_d) versus period for the box (top), beach (middle), and pipe (bottom) breakwaters. Results shown in full scale for a wave height of 1.15 m. Confidence intervals represented by vertical lines.

The increase in dissipation to 0.45 at a period of 5.9 s coincides with the reduced reflection at the same period (Figure 25 top panel). This could be the result of standing waves being formed in front of the breakwater. If these standing wave antinodes were not at a probe location then the full reflected amplitude may not have been captured. The

dissipation for the beach ranged from 0.93 to zero from periods 3.2 s to 7.8 s (middle panel Figure 27), respectively. This is likely because the slope to the beach is not long enough to allow longer period waves to shoal and break. The pipe has a maximum C_d of 0.50 at 3.2 s and drops to 0.31 at a period of 3.9 s (bottom panel Figure 27). The dissipation continues to drop to zero at a period of 5.9 s.

For the 2 m wave height cases, the increased wave reflection observed (Figure 26) resulted in negative values of dissipation for the box, which is a result of how the dissipation term is calculated. Provided that the enhanced reflected energy was related to resonance with both the basin and box, these negative values were taken as zero for the purposes of this comparison (Figure 28).

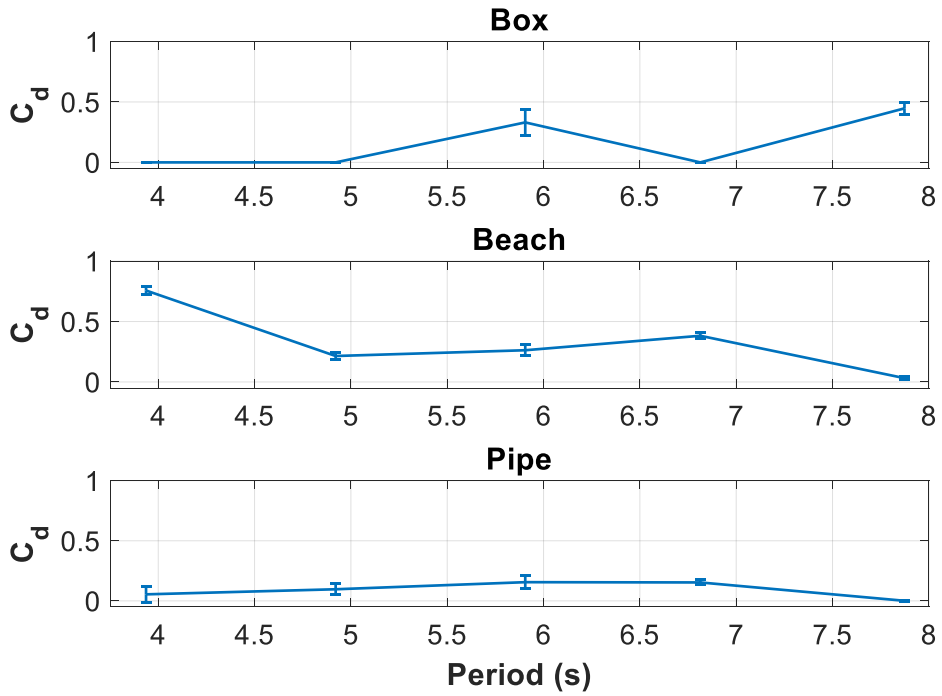

Figure 28. Dissipation coefficient (C_d) versus period for the beach (top) and pipe (bottom) breakwaters. Results shown in full scale for a wave height of 1.15 m. Confidence intervals represented by vertical lines.

The box breakwater had an increase to 0.33 at a period of 5.9 s, similar to the increase in the 1.15 m wave height at the same period to a C_d of 0.45. This increase occurring at the

same period as the smaller wave height case supports the previous assumption that a standing wave could have caused the full reflected wave height to not be captured. A standing wave would occur in the same location, with a different magnitude, for waves of the same period regardless of wave height.

At the smallest period of 3.9 s the beach breakwater had its maximum dissipation of 0.75 (top panel Figure 28). The C_d then decreased to 0.21 by a period of 4.9 s before increasing to 0.38 at a period of 6.8 s. The C_d then approached zero at a period of 7.9 s. The C_d at a period of 3.9 s was 20 % greater for the higher wave case of 2 m. This is most likely due to the increased steepness of the wave from the higher wave height, which would induce more breaking. The pipe breakwater's dissipation increased from zero at a period of 3.9 s to 0.16 at a period of 6.8 s (bottom panel Figure 28). The C_d then approached zero at a period of 7.9 s.

3.4. Mooring Forces

Mooring forces are an important aspect of floating breakwater design, because they dictate the design of the anchor. This research seeks to create designs that are easily deployed and the mooring forces exhibited by the designs will have a direct impact on the complexity of the mooring/anchor system. The windward mooring forces for the beach and box breakwater generally increased with the larger wave height, as expected (Figure 29).

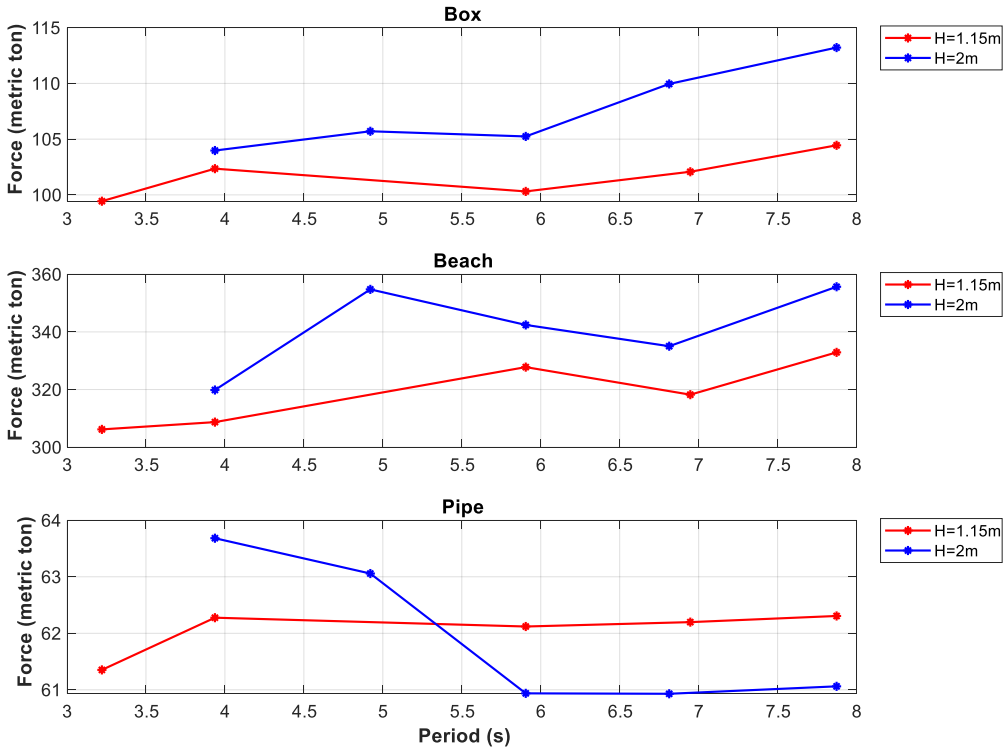

Figure 29. Full-scale windward mooring forces for the box (top), beach (middle), and pipe (bottom) breakwaters. The red line is the 1.15 m wave height and blue is the 2 m wave height.

The box had a peak mooring force of 113 metric tons at a wave height of 2 m and a period of 7.8 s (Figure 29 top panel). The beach breakwater experiences the largest mooring force, with a peak of 355 metric tons at a wave height of 2 m and a period of 7.8 s (Figure 29 middle panel), which is three times the maximum force experienced by the box. The pipe breakwater however, only experienced a maximum force of 63 metric tons with a wave height of 2 m at a period of 3.9 s (Figure 29 bottom panel). The increase in wave height from 1.15 m to 2 m caused an average increase of 6% in the mooring force for the box and beach breakwaters. The pipe breakwater mooring force did not vary more than 2% throughout the range of periods and wave heights. An increase in period resulted in an increase on the mooring forces for the box and beach breakwaters, increasing it by

approximately 10% from the range of 3.2 – 7.8 s. The recorded mooring line forces were broken down to anchor forces in global coordinates (Figure 30).

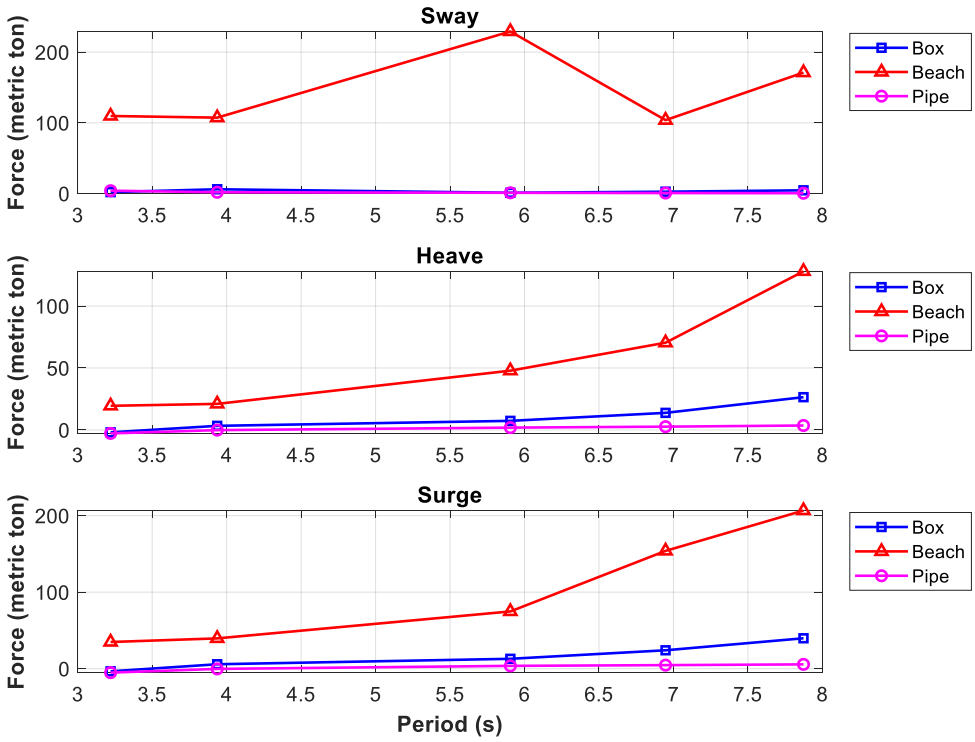

Figure 30. Maximum combined windward global anchor forces versus period in sway (top), heave (middle), and surge (bottom) degrees of freedom for the box (blue), beach (red), and pipe (magenta) breakwaters. Results in full scale for wave height 1.15 m.

The directions of the global forces are labeled using motion response directions to make it coincide with the global motion of the breakwater. The sway direction is the positive y direction (Figure 17), the heave is the positive z direction, and the surge is the positive x direction (direction of the wave field). The values are the total maximum force in the respective direction, the maximum for mooring 1 plus mooring 2. In the sway component the box and pipe breakwaters never exceed 7 metric tons, while the beach breakwater experiences a peak of 229 metric tons at a period of 5.9 s (Figure 30 top panel). In the heave direction the beach is again the highest, increasing from 19 to 128

metric tons over the range of periods (Figure 30 middle panel). The box breakwater does increase over the range of periods as well in heave, from 0 to 40 metric tons, while the pipe breakwater does not exceed 5 tons. In the surge direction, the beach increases from 35 to 207 metric tons as the period increases. The box increases from 0 to 40 metric tons and the pipe breakwater has a peak of 6 metric tons at a period of 7.8 s.

The forces in the heave and surge direction for the beach begin to increase exponentially as the wave period increases. This should be paid close attention as the natural wave environment may have periods greater than 8 seconds, which could cause failure in the moorings. The global values give the forces required by all the anchor points. These data would be important for determining how many anchor points are required based on anchor characteristics. The forces would be divided by the number of windward anchors chosen to determine the forcing on the individual anchor.

The same overall patterns hold true for the 2 m wave height with a few exceptions. The peak force in the sway direction for the beach breakwater shifted from a period of 5.9 s to 4.9 s with the increase in wave height (Figure 31 top panel).

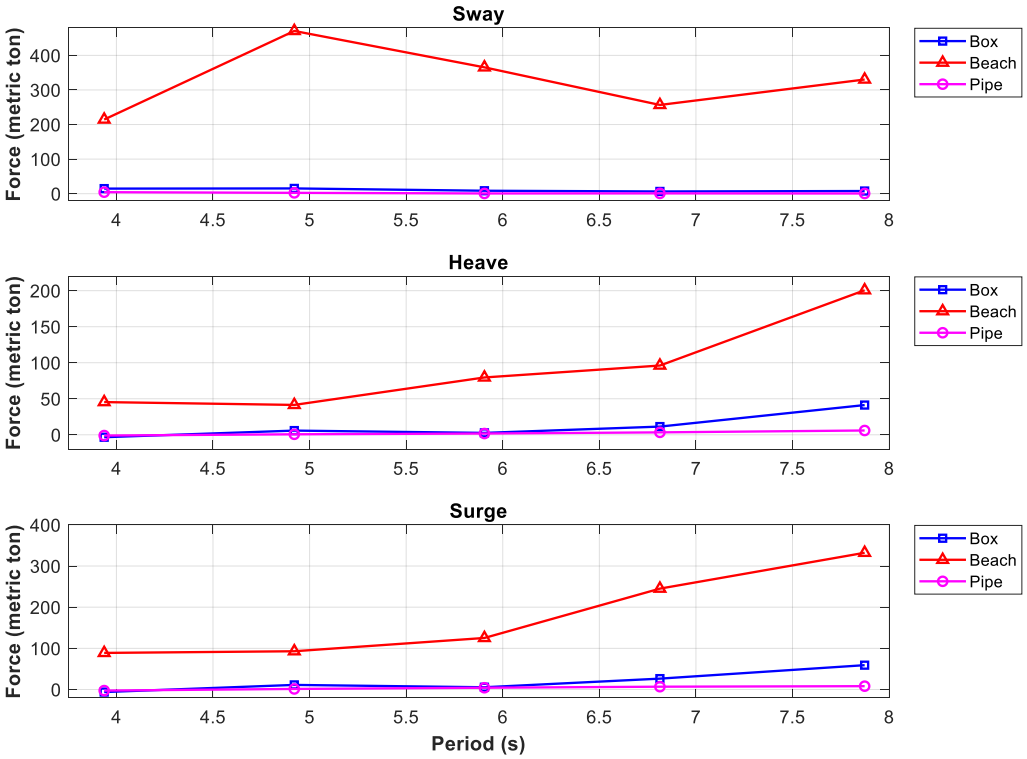

Figure 31. Maximum combined windward global anchor forces versus period in sway (top), heave (middle), and surge (bottom) degrees of freedom for the box (blue), beach (red), and pipe (magenta) breakwaters. Results in full scale for wave height 2 m.

This could be due to wave breaking being induced at a smaller period due to the larger wave height. The increased wave height from 1.15 to 2 m caused the forces to almost double for each breakwater at every period. This will have a significant impact on the design of anchors, as the wave heights may be larger than 2 m at times.

The movement of a floating structure in a wave environment is important for deployment and operation. Whether the structure is deployed to protect ships or the nearshore environment, knowing how far the breakwater will move from its original deployment is important. If too close, the breakwater could damage a ship while it is

offloading its cargo, or the breakwater could run aground if the movement brings it to a reef or much shallower waters. For these reasons, the motion responses are very important to any design. The motion responses were captured with the Qualisys motion tracking system for the surge and heave displacement, as well as the pitch rotation was compared for all three models for both the 1.15 m and 2 m wave heights (Figure 32 & Figure 33).

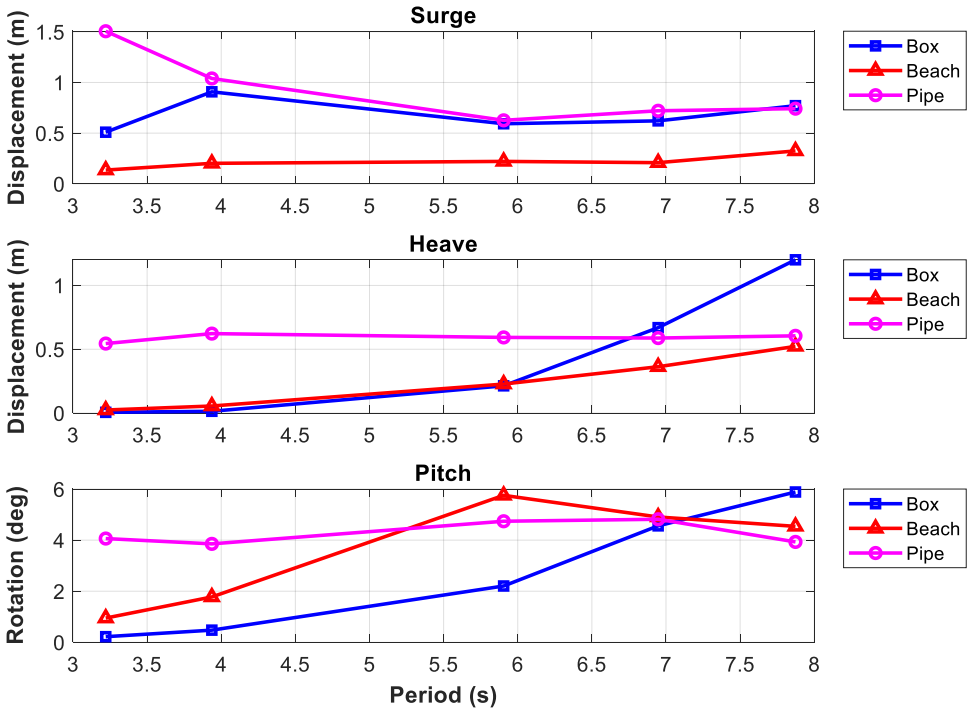

Figure 32. Surge (top), heave (middle), and pitch (bottom) motion response results for wave height 1.15 m versus period. The results are presented in full scale for the box (blue), beach (red), and pipe (magenta).

The beach breakwater's surge displacement remained consistent at 0.2 m throughout the range of periods, only increasing slightly when the period exceeded 7.5 s (Figure 32 top panel). This displacement was only a third of the box and pipe breakwaters. The box and pipe breakwater surge displacements converged to a displacement of 1 m at a period of 4 s and a displacement of approximately 1 m (Figure 32 top panel). These two breakwaters

remained around 0.6 m for larger periods. Although the pipe breakwater had a similar surge displacement to the box, the heave displacement for the pipe breakwater was the largest until a period of 6.75 s. The heave displacement for the pipe breakwater was consistently 0.6 m for the entire range of periods (Figure 32 middle panel). The beach and box breakwaters had a similar displacement of less than 0.3 m until the period of 6 s, which was less than half of the displacement of the pipe breakwater. At this period the box heave displacement rapidly increased by 1 m over the remaining two test cases and the beach displacement doubled to 0.5 m from a period of 6 to 8 s. Although the beach had the smallest displacements in both surge and heave, the beach rotated in pitch to a peak of 6 degrees. The beach also had greater pitch rotation than the box up to a period of 7 s and higher than the pipe breakwater from 5.5 to 7 s (Figure 32 bottom panel). The box's pitch response also varies with wave period, increasing slowly from 0 at a period of 3 s, to 6 degrees at a period of 8 s. While both the beach and box breakwater's pitch response changed with increasing wave period, the pipe breakwater consistently pitches at 4 degrees throughout the range of periods tested.

The three breakwaters exhibited similar patterns for the higher wave height of 2 m (Figure 33).

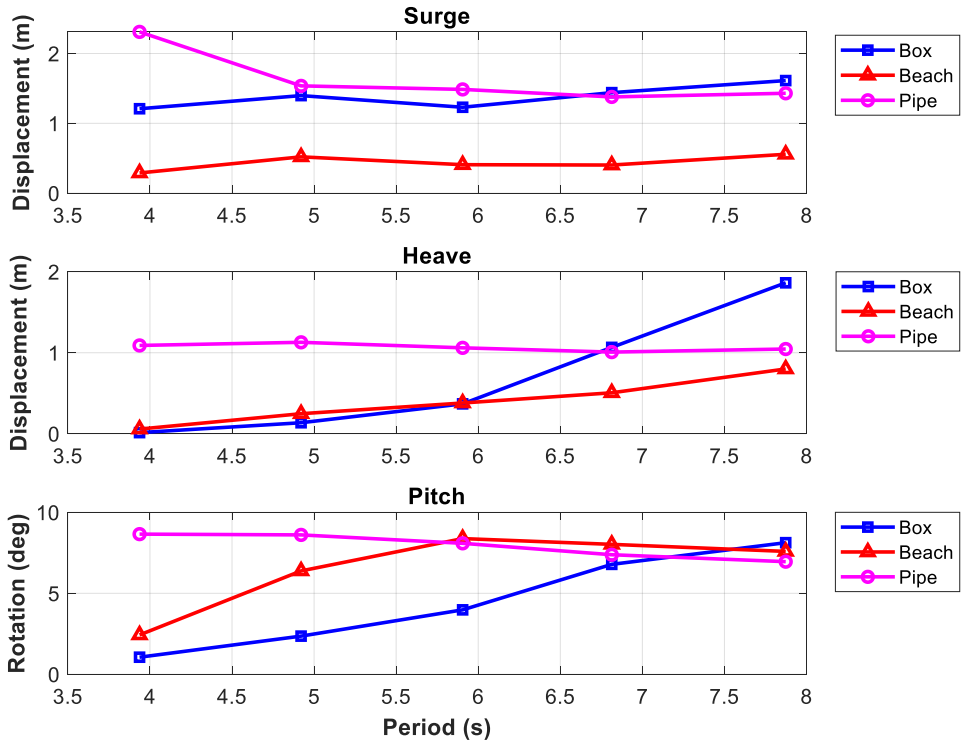

Figure 33. Surge (top), heave (middle), and pitch (bottom) motion response results for wave height 2 m versus period. The results are presented in full scale for the box (blue), beach (red), and pipe (magenta).

The surge displacements follow the same pattern, with an increased magnitude, as in the 1.15 m wave height, the pipe and box converging to a displacement of 1.5 m at a longer period of 5 s (Figure 33 top panel). The magnitude of the surge and heave displacements doubled for periods greater than 5 s. The beach surge response also doubled to a value of 0.4 m, which stayed consistent over the range of wave periods. The heave response doubled in magnitude for all three breakwaters (Figure 33 middle panel). The pipe remained around 1 m displacement for the duration of the wave periods, while the beach increased linearly as the wave period increased. The box rapidly increased in heave motion from a period of 6 s to 8 s, more than doubling in amplitude. The pitch response for the pipe breakwater doubled from 4 degrees to 8 degrees with the increased wave height. The magnitude of the rotation for the box and the beach increase by 1.5 times

from the small wave height to the larger wave height, with a maximum rotation of 8 degrees with the 2 m wave height (Figure 33 bottom panel).

CHAPTER 4
DISCUSSION

4.1. Relative performance of breakwaters

Three breakwaters were designed with lightweight composite sandwich material construction, in order to analyze if wave attenuation could be dominated by dissipation rather than reflection, while still obtaining an optimal energy reduction of 50 %. The percent of attenuation induced by dissipation is compared across breakwaters, in order to understand which structure was more effective at attenuating wave energy through dissipation mechanisms rather than reflection (Figure 34).

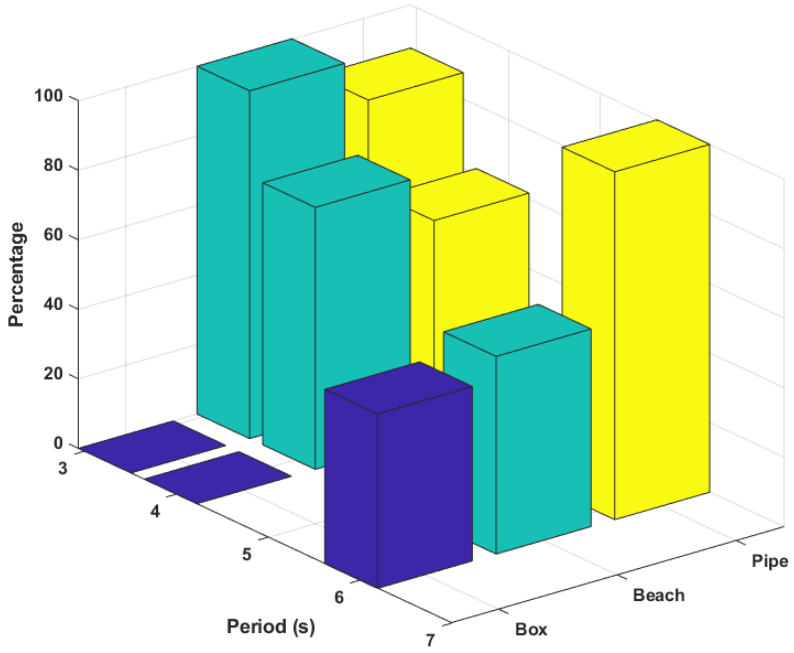

Figure 34. Percentage of attenuation that is dissipation for the box (blue), beach (green), and pipe (yellow) breakwaters. Results shown for 1.15 m wave height within operational (SS3) range.

The beach and pipe breakwaters were dominated by dissipation within the target sea state range (3-6 s). The percent of attenuation represented by dissipation for the beach

and pipe breakwater was greater than 75% for the periods of 3-4 s (Figure 34). At a period of 6 s the beach breakwater's dissipation drops to 56% of the attenuation while the pipe remained near 100%. The drop in the beach breakwaters dissipation occurs as the wave period and wavelength increase. As the waves become longer they become less steep and therefore less prone to wave breaking. For the beach to more effective in longer period waves, it would have to have a longer windward slope to increase the time for the wave to setup to induce breaking. The pipe remaining consistent coincides with the mechanism it employs to dissipate wave energy. The structure was not designed to have a significant reflecting surface, therefore the dominant mechanism should be dissipation throughout the range of periods. Increasing the wave period should not affect the drag and vortex shedding induced by the pipes until the structure motion coincides with the wave field (riding the waves). In this experiment the structure began to ride the waves around a period of 3.5 s and therefore the dissipation remained relatively constant. The box however, was dominated by reflection with no attenuation due to dissipation until a period of 6 s (Figure 34). Once the box reached a period of 6 s the attenuation due to dissipation increased to 50%. This is likely due to a standing wave being formed as discussed in section 3.3 as the box primarily utilized reflection as its attenuation mechanism.

The box attenuated the most wave energy, exceeding the goal of a $C_t < 0.5$ until a wave period of over 7 s for both wave heights. The beach featured a $C_t < 0.5$ until a wave period of 5.5 s for both wave heights, while the pipe breakwater only exceeded $C_t < 0.5$ at wave period of 3.5 s for the smaller wave height case. All three breakwaters became less effective at attenuating wave energy as the wave period increased, which is typical of

floating breakwaters. The box attenuated the most energy by primarily utilizing reflection. This demonstrated the effectiveness of reflection as a wave attenuation mechanism. As the wave period approached 8 s, the box began to ride the waves which diminished the capacity for reflection. The pipe breakwater was only able to generate enough dissipation to attenuate below 0.5 for the smaller wave periods (< 3.5 s) with the 1.15 m wave height. This is largely due to the pipe breakwater riding the waves. The beach primarily utilized dissipation as the attenuation mechanism while attaining similar results as the reflecting box up to a period of 5.5 s. The effectiveness of the beach in the smaller period wave cases is assumed to be due to the dissipation mechanism induced by wave breaking. The smaller period waves have a greater steepness than the longer period waves of the same wave height and thus are closer to their breaking point. This coupled with the semi-taut mooring system to resist moving with the waves, allowed waves to break on the beach breakwater.

Forces in the beach breakwater mooring lines were three times larger than the forces in the lines of the box breakwater, in order to limit the motion response of the beach. An analysis of the location of the mooring line attachments to the beach breakwater could help reduce the pitch motions that were visible during testing. The beach rotated in pitch as much as 6-8 degrees, and if this were reduced further, the beach could be more effective at attenuating wave energy. The beach mooring lines restricted the movement in surge and heave to under a meter at full scale for all wave cases. The trade off to restricting the motion was large mooring line forces experienced with the beach breakwater of over 300 metric tons. The magnitude of these mooring forces will require special consideration when determining the type of anchors required.

The pipe breakwater's minimal weight resulted in a natural period in heave of 3.18 s which caused it to ride the waves for most of the wave cases. This resulted in poorer performance than was anticipated. This performance could be enhanced by stiffening the mooring lines to be similar to a semi-taught system, or increasing the added mass. For example, two wave cases (not shown) were run using the box mooring lines with the pipe model and the attenuation was increased by 5-8%, which suggests that increasing the stiffness would increase the attenuation of the pipe breakwater. One advantage of the pipe breakwater in terms of installation was that it was eight times lighter than the beach breakwater and had a heave stiffness almost four times smaller than the box breakwater. This caused the heave natural period to be 3.18 s at full scale, which was close to the smallest wave period tested (3 s full scale). Once the wave environment surpassed this period, the pipe breakwater rode the waves. This still allowed the flow to pass through the pipes, creating vortices, which accounted for the small amount of attenuation recorded. The attenuation could be improved by increasing the stiffness in the mooring lines or making the trapezoidal float narrower, thus reducing the water plane area. Varying the diameter of the pipes to increase the range of the vortex shedding frequencies and a second or third row of pipes could also increase the drag and potential for forming vortices.

The reflection was over four times larger in the box breakwater than in the beach or pipe breakwaters. The reflection induced by the box breakwater led to increased wave activity in the basin, making accurate computations difficult. These disruptive reflected waves are also an indication of a disadvantage of the box breakwater, or any breakwater

that largely utilizes reflection. Reflected wave energy can be detrimental to navigation, recreation, and erosion in the surrounding areas due to the increased energy.

Despite the beach having a large reflective surface in the front of the breakwater, it produced very little reflection (Figure 25 & Figure 26). This is because the majority of the reflective face is below the area of greatest wave energy. The reflection by the beach and pipe breakwaters provide the added benefit of reduced destructive reflected wave energy.

The size of the breakwater is important due to the increased cost for more materials and for logistics of transportation and deployment. The breakwaters may need to be initially transported on land, which limits the size based on the capacity of flatbed trucks. Once in the water, the breakwater needs to be towed to the location of installation. This process will be easier and less expensive for smaller structures, especially if several are needed to form an array for coastal protection. The beach breakwater encompassed half of the footprint of the box. Despite this, the beach performed as desired for the majority of the target wave environment. With the reduced size, 8 m wide opposed to 16.9 m wide, the beach would be easier to move and deploy. The freeboard of 0.8 m versus the box at 3.6 m would also be desirable for coastal communities, as it would reduce the amount of visible obstruction and have a smaller impact on the view.

4.2. Design Disadvantages

The natural period of the box caused some additional excitation in the basin during testing. The heave (7.89 s) and pitch (7.70 s) natural periods were both close to the last wave period tested (7.87 s). The natural period for the box and the pipe model was calculated using data from the free decay tests. The free decay was performed a minimum of 3 times with the results averaged. The box in heave for example was pushed down and

released. As the box moved up and down vertically, the motion was captured using Qualisys Motion Tracking Software (Figure 35).

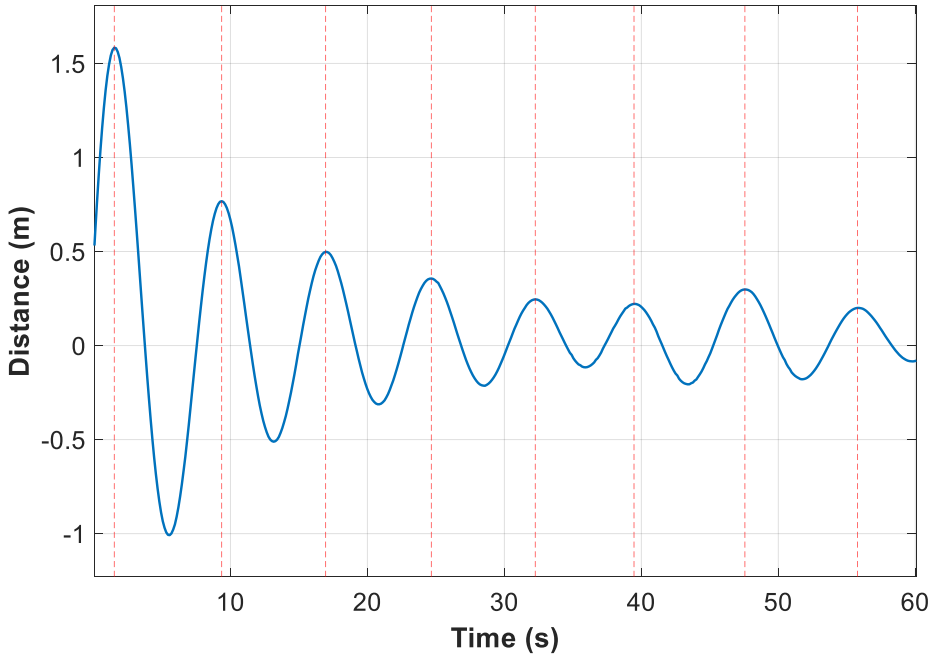

Figure 35. Heave free decay test for the box (in blue). Red dashed vertical lines mark the peaks of displacement. Dimensions are in full scale.

The time from the first peak to the last peak was divided by the number of oscillations (number of peaks – 1). This resulted in the natural period for this run.

The beach design also has the disadvantage of diminished performance with large water level fluctuations, for example, alarge tidal range. The taught mooring lines will not allow the structure to rise with the rising tide, resulting in less exposed structure, which will limit wave breaking capabilites.

4.3. Study Limitations

There are several limitations to this research. All test cases reported were monochromatic/ regular incident wave cases. The reflection, in particular, can be amplified by monochromatic waves, as standing waves can be formed due to the incident

and reflected waves having the same period. The natural coastal environment consists of incident irregular wave trains as opposed to the incident regular waves used in this study. The natural environment also consists of directionally changing incident waves and in this study only waves propagating normal to the breakwaters were considered. The directionality and irregularity of the incident wave trains would have a different effect on the attenuation of the breakwaters. The performance of the breakwaters may differ slightly with the experimental results due to the scaled depth. The breakwaters are designed to be deployed in depths of 20 m and the scaled depth of the test basin was 180 m. In a shallower water environment, the breakwaters should perform better, especially the beach breakwater. As a wave approaches the shore the wave height increases and the wave length remains the same, the closer the ratio of the wave height to the wave length comes to 1/7, the closer the wave is to breaking. Therefore, a shallower environment would enable the beach breakwater to induce more wave breaking, increasing the dissipation and the attenuation performance.

4.4. Lessons Learned

While the reduction in weight for the breakwater designs would be beneficial for deployment and relocation, it created enhanced structural motions during testing. The natural period (T_o) of the structure can be found for each degree of freedom using the following equation.

$$T_o = 2\pi \sqrt{\frac{m + m_a}{k_{dof}}} \qquad [17]$$

Where m is the structural mass, m_a is the added mass, and k_{dof} is the combined system stiffness in the corresponding degree of freedom. Reducing the structural mass reduced the natural period, which resulted in the natural period being closer to the incident wave periods. Methods to increase the added mass without significantly increasing the overall mass should be considered, this includes the addition of sub-surface heave plates. The increase in added mass would result in an increase in the natural period to outside the expected wave environments, greater than 15 s. The stiffness could also be increased until the system functions as a semi-taught system. The goal would be to reduce the natural period below the target environments, less than 2 s.

The high stiffness in the taught mooring system for the beach resulted in mooring forces that were three times higher than the box breakwater. This would increase the cost and complexity of installation for the beach breakwater. If the stiffness in the lines were reduced, the forces in the lines would decrease. If this could be done while maintaining the effectiveness of the beach at attenuating wave energy, this would make the system more cost effective and easier to deploy.

Testing of any floating structures has many challenges. In this test campaign, challenges arose from the natural frequency of the basin, the structures, and structure induced reflection. Special care needs to be taken, prior to conducting experiments, to analyze the fundamental dynamic characteristics of the test environment. The environmental producing capability of the wave maker is important and often one of the first factors considered for scaling purposes. The dynamic response of the facility also needs to be considered in an effort to avoid the natural frequencies of the facility. This

has the potential to be overlooked and could adverse effects, as it did in this series of experimentation.

The testing of a highly reflective structure can also pose challenges in a confined basin. Methods to reduce the reflection in the wave basin should be considered. There was significant reflection generated during the testing of the box breakwater, which helped excite the natural frequencies of the basin.

CHAPTER 5

CONCLUSIONS AND FUTURE WORK

5.1. Conclusions

This research aimed to: determine if floating breakwaters can be constructed out of lightweight materials and still be effective; measure the wave attenuation capacity and mooring forces associated with the breakwaters; and to determine if turbulence generation could be used to ensure dissipation was the primary attenuation mechanism. A summary of key parameters from this research are shown in Table 2.

Table 2. Full-scale parameters for the box, beach, and pipe breakwaters. Experimental results shown for wave height 1.15 m and a period of 3.9 s.

	Breakwater Design		
Parameter	**Box**	**Beach**	**Pipe**
Width (m)	16.9	8.56	8
Length (m)	40	40	40
Height (m)	12.1	12	12
Structure mass (mt)	200.9	1,160.30	47.6
Installed system mass (mt)	5,836.90	1,160.30	268.9
Operational ballast mass (mt)	5,636.10	0	221.3
CG from keel (m)	4.44	3.77	8.32
CB from keel (m)	4.21	4.87	7.99
Draft (m)	8.42	11.19	8.99
Freeboard (m)	3.59	0.81	3.01
Hull displacement (m^3)	5,694	1,875	262
Structural heave stiffness (N/m)	6.80E+06	1.05E+06	1.77E+06
Structural pitch stiffness (Nm/rad)	8.93E+08	1.34E+08	2.35E+08
Structural roll stiffness (Nm/rad)	1.49E+08	1.13E+07	1.97E+06
Mooring system	Catenary	Taught	Catenary
Max mooring force (mt)	102.4	308.7	62.3
Ct	0.50	0.18	0.60
Cr	0.88	0.15	0.10
Cd	0.00	0.67	0.31
Max surge displacement (m)	0.90	0.25	1.1
Max heave displacement (m)	0.05	0.1	0.6
Max pitch response (deg)	0.05	1.9	4

Floating breakwaters constructed of lightweight materials can be effective at reducing an incident wave environment by utilizing dissipation as its primary attenuation mechanism, with the added benefit of having a 50% smaller structural footprint required than a reflective structure. The composite sandwich material allowed the designs to weigh 12% of the same designs in concrete, which allows for easier deployment. The drawback to the lighter structural design is the reduced structural natural period, which will require a mooring design that provides heave stiffness as well as a surge restoring force or additional added mass. The added heave stiffness is needed to prevent the breakwater from having a heave natural period near the period of the wave environment. The two test cases for the pipe breakwater that were run with the stiffer box mooring lines resulted in an attenuation increase of 5% to 8%, though, further investigation is required to confirm this trend.

The box attenuated 50% of the wave energy up to a period of 7 s, while the beach attenuated more than 50% of the energy up to a period of 5 s. The weakest attenuation was caused by the pipe breakwater, which only attenuated 50% of the energy up to 3.5 s period. The mooring forces for the breakwaters are useful to understand anchor and mooring line design for future applications. The pipe breakwater had the smallest maximum windward mooring force of 63.8 metric tons; the box had a maximum of 113 metric tons and the beach a maximum of 355 metric tons. The box and pipe breakwaters could be installed using typical catenary mooring lines, however the beach would need a taut system to be installed which would add to the cost of the project. The deployment and installation of the beach breakwater requires special consideration due to the large mooring forces from the required pre-tension in the lines.

The pre-tension contributed to the beach's ability to attain wave attenuation similar to the box within the target wave environments (3 – 6 s). The beach breakwater was successful at utilizing a wave attenuation mechanism alternative to reflection while reducing the size of the structure. The beach employed turbulence generation via wave breaking, which resulted in energy dissipation. As shown in Figure 34, the beach used dissipation as its primary mechanism, which allowed for the reduced footprint, being half the size of the box breakwater.

Alternative wave attenuation mechanisms can be as effective as traditional reflection while reducing the size of the structure. Special consideration needs to go into the design and application of the mooring system, as it can have a large impact on overall performance. Floating breakwaters that are lighter may be easier to transport and deploy, but will require moorings that keep the structural natural periods away from the expected environmental periods. A cost analysis should be conducted to determine the most practical design.

5.2. Future Work

Future work will include comparing the beach breakwater to an additional design that will be suspended in the water column. The suspended design will consist of 3D printed porous screens that will expand on utilizing dissipation as a primary attenuation mechanism by creating turbulence as the wave passes through the holes. The design will be optimized using a computational fluid dynamics (CFD) model, which will include evaluating the role of porosity (of screens and top of beach), size (including draft required and slope of beach), and mooring stiffness on wave attenuation. This work contributes to the overarching goal of designing an effective breakwater technology that

can be easily deployed and utilizes dissipation as a wave attenuation mechanism that can be used for nearshore coastal protection.

REFERENCES

Allyn, N., Watchorn, E., Jamieson, W. W., & Yang, G. (2004). Port of Brownsville Floating Breakwater. *Proceedings of Ports Conference 2001* (pp. 1-10). ASCE.

Anis, A., & Moum, J. N. (1995). Surface Wave-Turbulence Interactions: Scaling e(z) near the Sea Surface. *American Meteorological Society*, 2025-2045.

Bridon-Bekaert Ropes Group. (2018). *Moorline Polyester.* Brussels: Bridon-Bekaert Ropes Group.

Briggs, M. J. (2001). *Performance Characteristics of a Rapidly Installed Breakwater System.* U.S. Army Engineer Reseach and Development Center. Vicksburg: Coastal and Hydraulics Laboratory .

Carr, J. H. (1951). Mobile Breakwaters. *Proceeding of 2nd Conference on Coastal Engineering*, (pp. 281-295). Houston.

Chen, G., & Belcher, S. E. (1999). Effects of Long Waves on Wind-Generated Waves. *Journal of Physical Oceanography, 30*, 2246-2256.

Christensen, E. D., Bingham, H. B., Friis, A. P., Larsen, A. K., & Jensen, K. L. (2018). An experimental and numerical study of floating breakwaters. *Coastal Engineering*(137), 43-58.

Dai, J., Wang, C. M., Utsunomiya, T., & Duan, W. (2018). Review of recent research and developments on floating breakwaters. *Ocean Engineering*, 132-151.

Davidson, P. A. (2015). *Turbulence - An Introduction for Scientists and Engineers.* Oxford University Press.

Det Norske Veritas. (2010). *Recommended Practice DNV-RP-C205: Environmental Conditions and Environmental Loads.*

Emery, W., & Thompson, R. (2014). *Data Analysis Methods in Physical Oceanography*. Waltham: Elsevier.

Giles, M. L., & Sorensen, R. M. (1978). *Prototype Scale Mooring Load and Transmission Tests for a Floating Tire Breakwater.* Fort Belvoir: U.S. Army Corps of Engineers Coastal Engineering and Research Center.

Hales, L. Z. (1981). *Floating Breakwaters: State of the Art Literature Review.* U. S. Army Coastal Engineering Research Center. Fourt Belvoir: Technical Report 81-1.

He, F., Huang, Z., & Law, A. W.-K. (2012). Hydrodynamic performance of a rectangular floating breakwater with and without pneumatic chambers: An experimental study. *Ocean Engineering*(51), 16-27.

Headland, J. R. (1995). Floating Breakwaters. In G. Tsinker, *Marine Structures Engineering: Specialized Applications* (pp. 367-411). Springer US.

Huang, Z., He, F., & Zhang, W. (2014). A floating box-type breakwater with slotted barriers. *Journal of Hydraulic Research*, 720-727.

Hudson, R., Hermann, F., Sager, R., Whalin, R., Keulegan, G., Chatham, C., & Hales, L. (1979). *Coastal Hydraulic Models.* Vicksburg: U.S. Army Waterways Experiment Station.

Ji, C., Cheng, Y., Yang, K., & Oleg, G. (2017). Numerical and experimental investigation of hydrodynamic performance of a cylindrical dual pontoon-net floating breakwater. *Coastal Engineering*(129), 1-16.

Ji, C.-Y., Chen, X., Cui, J., Gaidai, O., & Incecik, A. (2016). Experimental study on configuration optimization of floating breakwaters. *Ocean Engineering*(117), 302-310.

Ji, C.-Y., Chen, X., Cui, J., Yuan, Z.-M., & Incecik, A. (2015). Experimental study of a new type of floating breakwater. *Ocean Engineering*(105), 295-303.

Kopp, R. E., Horton, R. M., Little, C. M., Mitrovica, J. X., Oppenheimer, M., Rasmussen, D., . . . Tebaldi, C. (2014). Probabilistic 21st and 22nd century sea-level projections at a global network of tide-gauge sites. *Earth's Future*(2), 383-406.

Lochner, R., Faber, O., & Penney, W. G. (1948). *The Bombardon Floating Breakwater: The Civil Engineer in War, Vol II.* London: Institute of Civil Engineers.

Mani, J. S. (1991). Desig of Y-Frame Floating Breakwater. *Journal of Waterway, Port, Coastal, and Ocean Engineering*(117(2)), 105-119.

McCartney, B. L. (1985). Floating Breakwater Design. *Journal of Waterway, Port, Coastal, and Ocean Engineering*(111(2)), 304-318.

Neelamani, S., & Ljubic, J. (2018). Experimental Study on the Hydrodynamic Performance of Floating Pontoon Type Breakwater With Skirt Walls. *Journal of Offshore Mechanics and Arctic Engineering, 140*, 1-9.

Pena, E., Ferreras, J., & Sanchez-Tembleque, F. (2011). Experimental study on wave transmission coefficient, mooring lines and module connector forces with different designs of floating breakwaters. *Ocean Engineering*(38), 1150-1160.

PIANC, P. I. (1994). *Floating Breakwaters A Practical Guide for Design and Construction.* Report of Working Group no. 13 of the Permanent Technical Committee II.

Seymour, R. J., & Hanes, D. M. (1979). Performance Analysis of Tethered Float Breakwater. *Journal of The Waterway Port Coastal and Ocean Division*, 265-280.

Sorensen, R. M. (2006). *Basic Coastal Engineering.* New York, NY: Springer Science + Business Media, Inc.

The SWAN team. (2006). *SWAN Technical Documentation.* Delft: Delft University of Technology.

United Nations. (2018). Review of Maritime Transport 2018. *United Nations Conference of Trade and Development* (p. 23). New York and Geneva: United Nations Publications.

Wang, H. Y., & Sun, Z. C. (2010). Experimental study of a porous floating breakwater. *Ocean Engineering*(37), 520-527.

Williams, A., Lee, H., & Huang, Z. (2000). Floating pontoon breakwaters. *Ocean Engineering*, 221-240.

Yan, L. (2015). Optimization test of the structural style of rectangular floating box breakwater. *8th International Conference on Intelligent Computation Technology and Automation*, (pp. 617-620).

APPENDIX: RESONANT BEHAVIOR IN THE BASIN

Upon investigation into the reflection values for the box exceeding one, it was determined that the natural resonant behavior of the basin as well as the box had an impact on the readings. The PSD for the box using probe 1 and the calibrated wave PSD were plotted with the closest natural frequencies of the box and the basin for a wave height of 2 m and a period of 3.9 s (Figure 36).

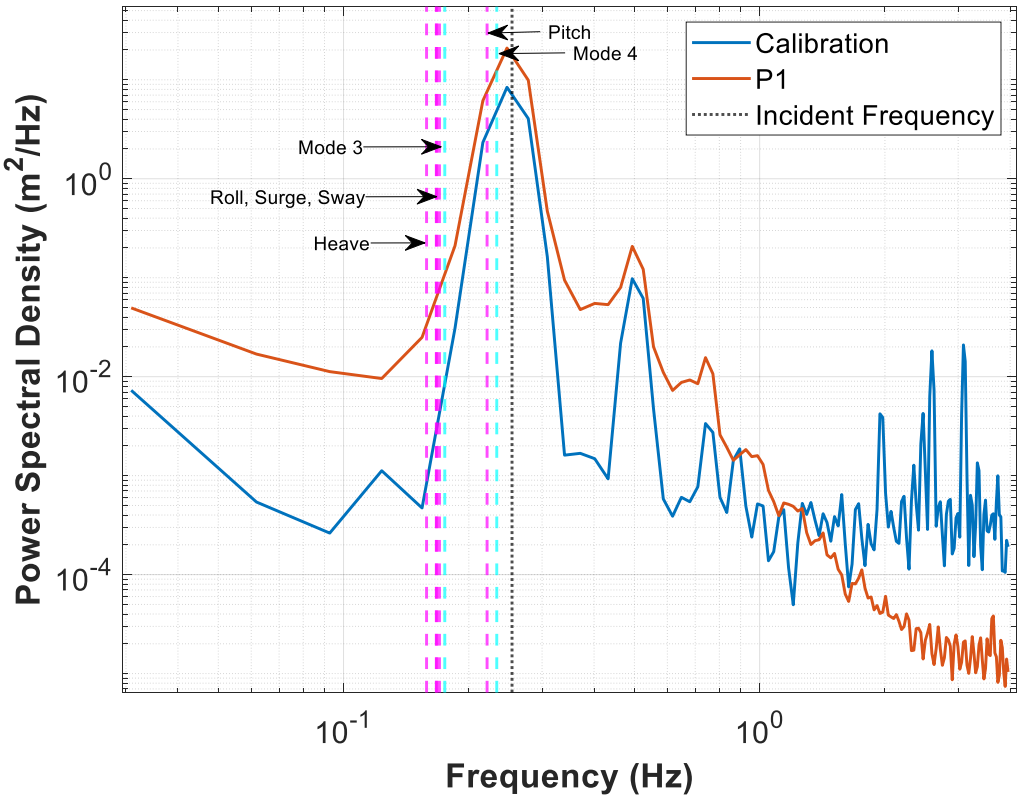

Figure 36. A loglog plot of the PSD for the calibration wave (blue) and wave probe 1 (red). The wave case had a wave height of 2 m and an incident wave period of 3.9 s (black dashed vertical line). The closest natural periods for the box (magenta) and the basin (light blue) are also plotted.

In this case only the box pitch natural frequency and the fourth mode of the basin were close to the incident frequency. The distribution of the peak power still is relatively narrow as would be expected. However, the peak is slightly shifted in the direction of the

natural frequencies. This shows that the natural frequencies are having some impact on the results.

The larger periods start being impacted by the box and basin more as the energy shifts to smaller frequencies. For a wave height of 2 m and a period of 4.9 s the impact is more prominent (Figure 37Figure 37).

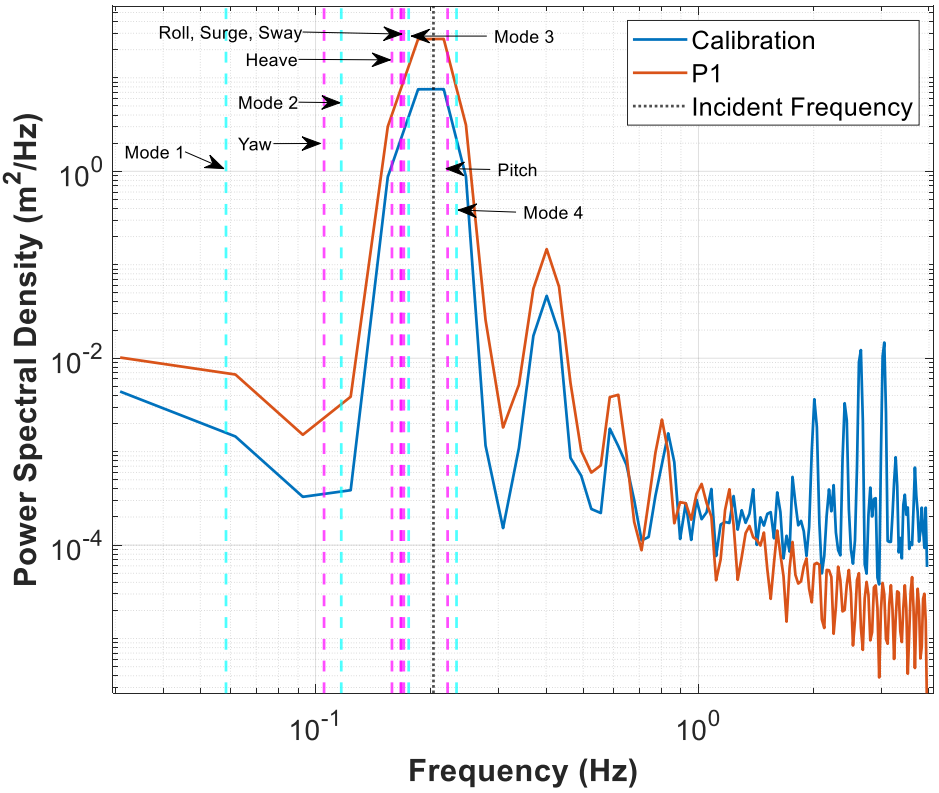

Figure 37. A loglog plot of the PSD for the calibration wave (blue) and wave probe 1 (red). The wave case had a wave height of 2 m and an incident wave period of 4.9 s (black dashed vertical line). The closest natural periods for the box (magenta) and the basin (light blue) are also plotted.

The incident frequency is now in between the pitch/mode 4 and the roll, surge, sway, heave, and mode 3. The distribution of the peak power is now wider than in Figure 36. The natural frequencies on both sides of the incident frequency have widened the peak. The shape and widening for the incident (calibrated) run is similar to the data from probe

1 at the area of the most energy. This implies that the basin natural frequency had a significant impact on this result. If the box natural frequency drove the widening of the peak then the incident PSD would have a narrower peak.

This widening continues for the 2 m wave height and the 5.9 s period (Figure 38).

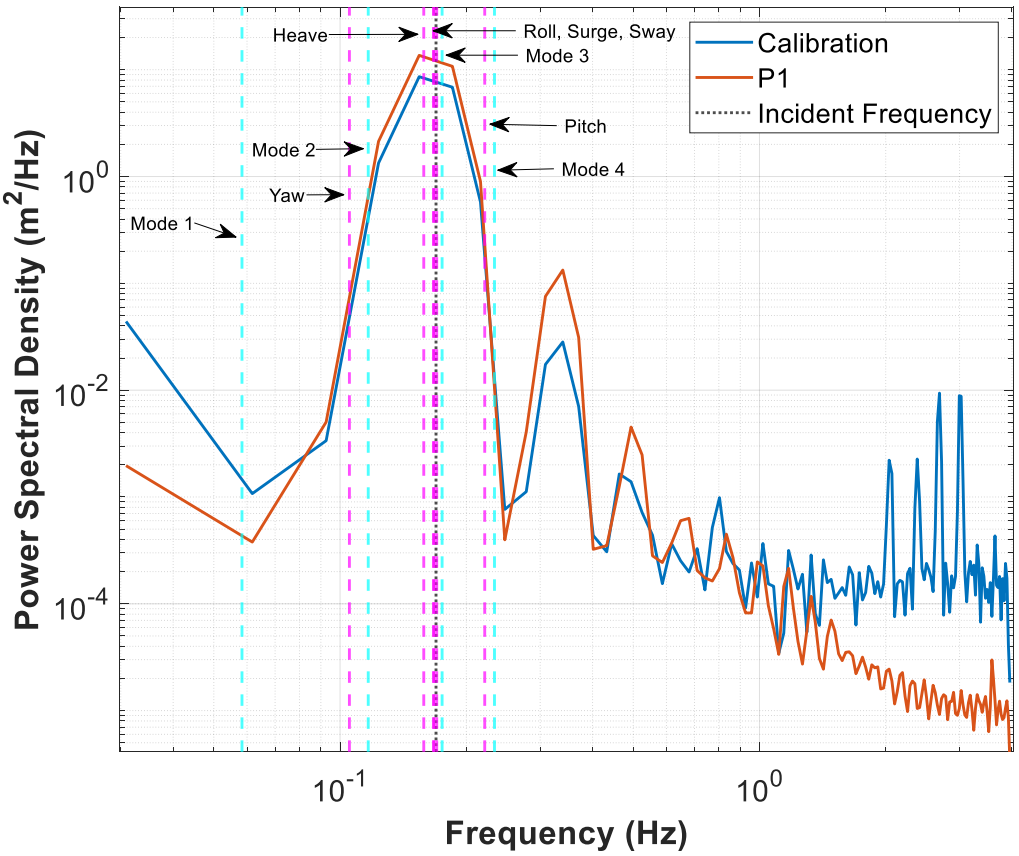

Figure 38. A loglog plot of the PSD for the calibration wave (blue) and wave probe 1 (red). The wave case had a wave height of 2 m and an incident wave period of 5.9 s (black dashed vertical line). The closest natural periods for the box (magenta) and the basin (light blue) are also plotted.

At a period of 5.9 s the peak is widened and slightly shifted to higher frequencies.

For a period of 6.8 s the peak is shifted to larger frequencies while the power distribution has remained widened (Figure 39).

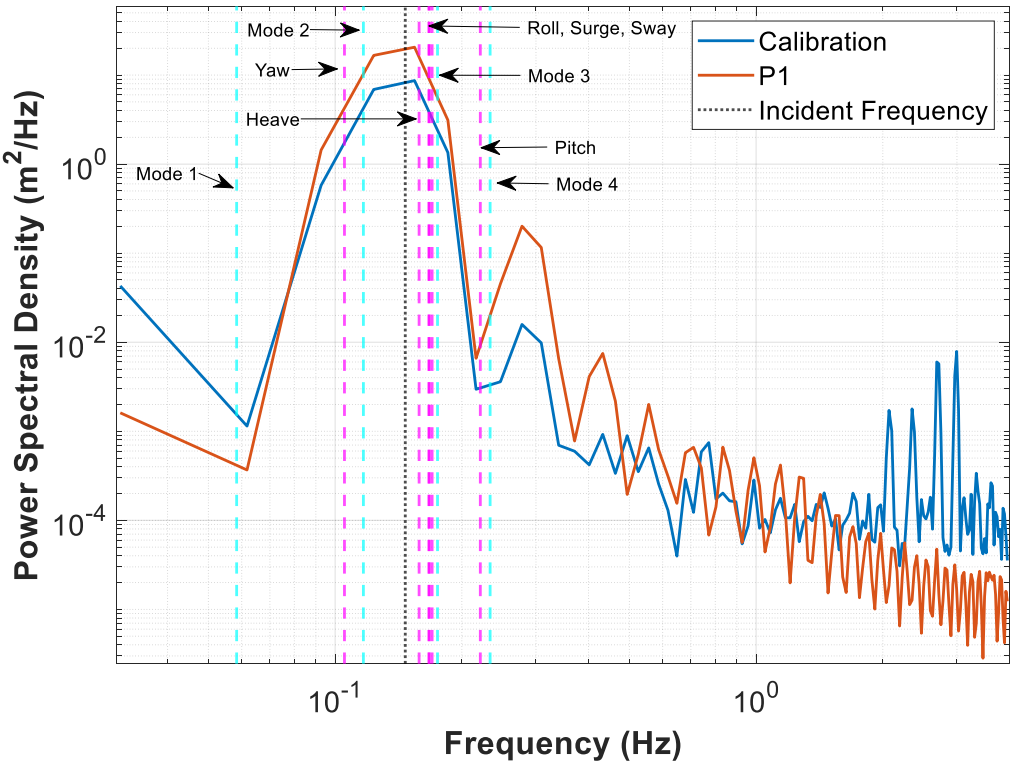

Figure 39. A loglog plot of the PSD for the calibration wave (blue) and wave probe 1 (red). The wave case had a wave height of 2 m and an incident wave period of 6.8 s (black dashed vertical line). The closest natural periods for the box (magenta) and the basin (light blue) are also plotted.

The incident wave frequency was close to the box heave frequency as well as basin mode 3, which pulled the peak to a larger frequency.

The largest period wave case run was 7.9 s at full scale. This brought the energy in the system closer the first mode of the basin (Figure 40).

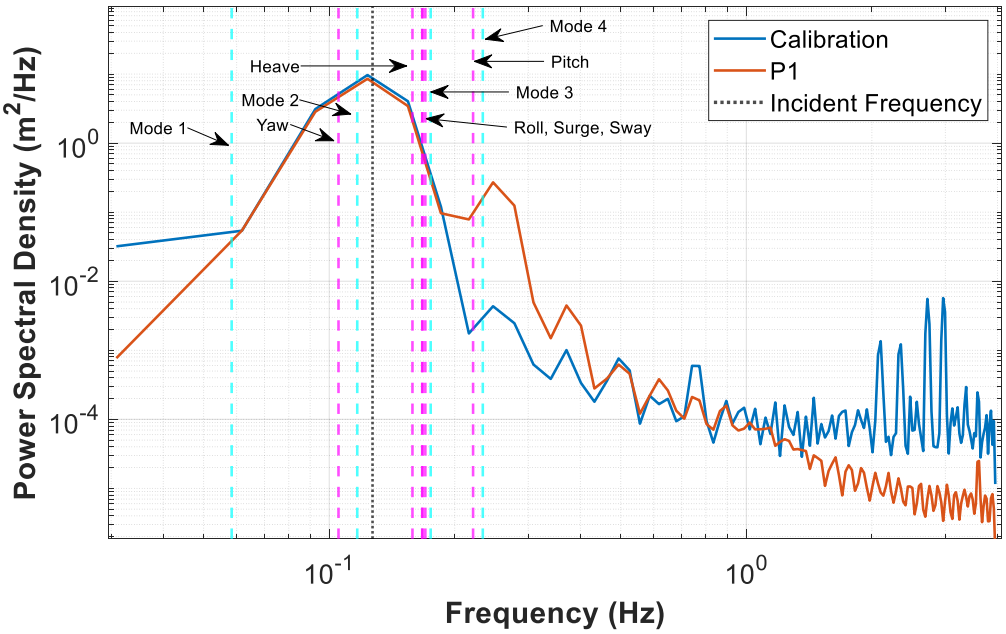

Figure 40. A loglog plot of the PSD for the calibration run (blue) and wave probe 1 (red). The wave case had a wave height of 2 m and an incident wave period of 7.9 s (black dashed vertical line). The closest natural periods for the box (magenta) and the basin (light blue) are also plotted.

This resulted in a significant widening of the power distribution from the incident frequency to the smaller frequencies. In future experiments, special care will be taken to avoid the modes of the basin.

BIOGRAPHY OF THE AUTHOR

Richard Perry was born in Lawrence, Massachusetts on August 31, 1979. He was raised in Kingston, New Hampshire and graduated from Sanborn Regional High School in 1997. He attended the University of Maine from the fall of 1997 to the spring of 2002. He then left the University and worked as a Retail Manager. In the fall of 2015 he returned to the University of Maine. He graduated with a B.S. in Civil Engineering from the University of Maine in the spring of 2018. Immediately following graduation, Richard entered the Civil Engineering graduate program through the Advanced Structures and Composites Center at the University of Maine. After receiving his degree, Richard will be staying at the Advanced Structures and Composites Center, as a research engineer, to begin his career in civil/coastal engineering. Richard is a candidate for the Master of Science degree in Civil Engineering from the University of Maine in December 2020.